Mutations in *twinstar*, a *Drosophila* Gene Encoding a Cofilin/ADF Homologue, Result in Defects in Centrosome Migration and Cytokinesis

Kristin C. Gunsalus,* Silvia Bonaccorsi,‡ Erika Williams,* Fiammetta Verni,‡ Maurizio Gatti,‡ and Michael L. Goldberg*

*Section of Genetics and Development, Cornell University, Ithaca, New York 14853; and ‡Centro di Genetica Evoluzionistica del CNR, and Dipartimento di Genetica e Biologia Molecolare, Università di Roma "La Sapienza", 00185 Roma, Italy

Abstract. We describe the phenotypic and molecular characterization of *twinstar* (*tsr*), an essential gene in *Drosophila melanogaster*. Two P-element induced alleles of *tsr* (tsr^1 and tsr^2) result in late larval or pupal lethality. Cytological examination of actively dividing tissues in these mutants reveals defects in cytokinesis in both mitotic (larval neuroblast) and meiotic (larval testis) cells. In addition, mutant spermatocytes show defects in aster migration and separation during prophase/prometaphase of both meiotic divisions. We have cloned the gene affected by these mutations and shown that it codes for a 17-kD protein in the cofilin/ADF family of small actin severing proteins. A cDNA for this gene has previously been described by Edwards et al. (1994). Northern analysis shows that the *tsr* gene is expressed throughout development, and that the tsr^1 and tsr^2 alleles are hypomorphs that accumulate decreased levels of *tsr* mRNA. These findings prompted us to examine actin behavior during male meiosis to visualize the effects of decreased twinstar protein activity on actin dynamics in vivo. Strikingly, both mutants exhibit abnormal accumulations of F-actin. Large actin aggregates are seen in association with centrosomes in mature primary spermatocytes. Later, during ana/telophase of both meiotic divisions, aberrantly large and misshaped structures appear at the site of contractile ring formation and fail to disassemble at the end of telophase, in contrast with wild-type. We discuss these results in terms of possible roles of the actin-based cytoskeleton in centrosome movement and in cytokinesis.

REGULATED interactions between actin and actin binding proteins provide an important structural basis for many cellular processes in eukaryotes, such as cell–cell adhesion, cell outgrowth and motility, muscle contraction, and cytokinesis. Changes in the intracellular localization and organization of actin are mediated by a repertoire of actin-associated proteins. These fall into several classes based on their effects on actin assembly and dynamics in vitro: proteins with cross-linking, bundling, capping, severing, polymerizing/depolymerizing, monomer sequestering, and motor activities have been described (reviewed by Vandekerckove and Vancompernalle, 1992). However, defining the role that each actin-associated protein plays in vivo and how multiple activities are coordinated remains a challenging task.

Proteins in the cofilin/actin depolymerizing factor (ADF)[1] family have been identified in a wide range of eukaryotic organisms, from yeast to plants to humans. These small molecular mass (15–20 kD) actin binding proteins constitute one of the two known classes of actin filament severing proteins; the other is comprised of the gelsolin/fragmin/villin-type proteins (see Vandekerckhove and Vancompernolle, 1992). In addition to severing, cofilin-like proteins also display actin filament and monomer binding activities in vitro. The properties of these proteins in vitro may be influenced by pH (Yonezawa et al., 1985; Hawkins et al., 1993; Hayden et al., 1993; Iida et al., 1993), the presence of membrane phospholipids (Yonezawa et al., 1990), other actin binding proteins (Nishida et al., 1984; Abe et al., 1990; Maciver et al., 1991), and in some cases, by phosphorylation of the protein itself (Morgan et al., 1993). These and other observations hint at how the activities of cofilin/ADF proteins might be regulated intracellularly.

Our current appreciation of the biochemical behavior of these molecules is not reflected by an understanding of the precise roles they play in vivo, although cofilin-like proteins are known to provide an essential function both in the yeast *Saccharomyces cerevisiae* (Iida et al., 1993; Moon et al., 1993) and in the nematode *Caenorhabditus elegans* (McKim et al., 1994). The yeast cofilin gene *COF1* is required for spore viability and growth, but the nature of the essential function or functions that are improperly per-

Address correspondence to Dr. M. L. Goldberg, Section of Genetics and Development, 425 Biotechnology Building, Cornell University, Ithaca, NY 14853. Tel.: (607) 254-4802. FAX: (607) 255-6249.

formed in the mutants is not known. In *C. elegans*, two slightly different cofilin-like proteins are generated by alternative splicing. A small deletion removing part of both transcripts is lethal (McKim et al., 1994); other mutations apparently affecting only one transcript are viable and result in paralysis and disorganized muscle filaments (Waterston et al., 1980; McKim et al., 1988). Vertebrates carry at least two distinct members of this family, cofilin and ADF/destrin, which differ both in their biochemical properties in vitro and in their expression patterns in different tissues and developmental stages (Bamburg and Bray, 1987; Matsuzaki et al., 1988; Abe et al., 1990; Moriyama et al., 1990*a*). Both porcine cofilin and destrin cDNAs can rescue the viability of *S. cerevisiae cof1* mutant spores (Iida et al., 1993). Thus, the biochemical differences seen in vitro between these proteins is insignificant for yeast cells, but multicellular eukaryotes may still require independent functions supplied by two or more members of the cofilin gene family.

In this paper, we describe both the molecular analysis of the *Drosophila* gene *twinstar* (*tsr*), which encodes a cofilin/ADF homologue, and the phenotypic consequences of mutations in this gene. Animals mutant for *tsr* die at the larval-pupal boundary and exhibit frequent failures in cytokinesis in both mitotic and meiotic cells. In addition, they show abnormalities in centrosome migration to the opposite ends of spermatocyte nuclei during the two meiotic divisions. These defects appear to be related to dramatic changes observed in the actin cytoskeleton in mutant spermatocytes.

Materials and Methods

Drosophila Stocks

The *twinstar*^{1} (*tsr*^{1}) allele was generated in a P element screen in the laboratory of Dr. J. Merriam (University of California, Los Angeles, CA) by the transposition of the single, marked P element pLacA92 (O'Kane and Gehring, 1987). The *tsr*^{2} allele was identified by Dr. Trisha Wilson (Stanford University, Palo Alto, CA) by screening a different collection of mutations induced with the marked P element P-*lacW* (Bier et al., 1989). Both alleles were maintained as heterozygotes balanced either by the second chromosome balancer *CyO* or by *TSTL*^{14}, a translocation between *CyO* and the third chromosome balancer *TM6B* (see Gatti and Goldberg, 1991). The deficiency strains *Df(2R)or*$^{BR\text{-}6}$, *Df(2R)or*$^{BR\text{-}11}$, and *Df(2R)G10-BR-27* were constructed and kindly provided by Dr. Bruce Reed (Whitehead Institute, Cambridge, MA). The latter deletion is associated with an inversion, *In(2LR)lt*^{G10L}*BR-27*^{R}, constructed using autosynaptic elements (see Gubb et al., 1988). *Df(2R)bw*^{S46} is described in Simpson (1983).

Germline Transformation

The 6.4-kb genomic fragment shown in Fig. 7 *A* (RS6.4) was subcloned from Bluescript KS II^{+} (Stratagene Inc., La Jolla, CA) into the transformation vector pW8 (Klemenz et al., 1987) using the NotI and XhoI sites present in both polylinkers. This putative pW8-*tsr*$^{+}$ construct was injected into *w;Sb e [Δ2-3]/TM6* embryos, which supply the transposase required for P element transposition (Robertson et al., 1988). pW8 carries a mini-*white*$^{+}$ gene as a selectable marker. Survivors were mated individually to *z*^{1} *w*^{11e4} (Lindsley and Zimm, 1992), and progeny were screened for transmission of the *w*$^{+}$ eye color. Several lines carrying independent insertions of pW8-*tsr*$^{+}$ were recovered. One of these lines carried a nonlethal insertion of pW8-*tsr*$^{+}$ on the third chromosome that was able to rescue the lethal, mitotic, and meiotic phenotypes of both *twinstar* alleles when present in either one or two copies. Stocks homozygous for [pW8-*tsr*$^{+}$] and either *tsr*^{1} or *tsr*^{2} were established; Southern analysis of genomic DNA confirmed the presence of *tsr* mutant alleles and *tsr*$^{+}$ transgenes in these lines (data not shown).

Cytology

Larval Neuroblasts. Homozygous *tsr* larvae were selected from stocks or crosses in which mutant *tsr* alleles were balanced over the *TSTL*^{14} translocation. Because this balancer carries the dominant larval marker *Tubby* (*Tb*), homozygous mutant individuals (phenotypically non-*Tb*) can be unambiguously distinguished from heterozygous *tsr/TSTL*^{14} larvae (phenotypically *Tb*). Mutant and control brains were dissected, fixed, and squashed in aceto-orcein according to our usual procedure (Gatti and Goldberg, 1991). To estimate the mitotic index of *tsr* mutants relative to controls, we determined the average number of mitotic figures per optic field in control (Oregon R) and mutant brain squashes (Gatti and Baker, 1989). The optic field chosen for this analysis is the circular area defined by a phase-contrast Neofluar 100× oil-immersion Zeiss objective, using 10× oculars with the Optovar set at 1.25× (Carl Zeiss, Inc., Thornwood, NY).

Larval Testes. To examine spermatid morphology in live material, larval testes were dissected in testis isolation buffer (183 mM KCl, 47 mM NaCl, 10 mM Tris-HCl, pH 6.8) and gently squashed in 2 μl of the same buffer under a 20 × 20 coverslip. These live preparations were immediately scored by phase contrast microscopy.

Two different procedures were used for cytological analysis of fixed testes. For simultaneous tubulin immunostaining and Hoechst 33258 staining, testes were fixed and processed as described by Cenci et al. (1994); tubulin was detected using an anti–α-tubulin Ab raised against chick brain microtubules (Amersham Corp., Arlington Heights, IL; Blose et al., 1982). For simultaneous visualization of chromatin, microtubules, and F-actin, testes squashes were prepared according to Cenci et al. (1994), but after freezing in liquid nitrogen and removal of the coverslip, squashes were fixed for 10 min by immersion in ethanol precooled at −20°C, followed by a 7-min treatment with freshly made 3.7% formaldehyde in PBS. Slides were then washed two times in PBS (5 min each) and immersed for 30 min in PBT (PBS + 0.1% Triton-X 100). After this treatment, they were incubated for 1 h with anti–α-tubulin monoclonal Ab diluted 1:50 in PBS, washed two times in PBS (5 min each), and then incubated for 1 h with the secondary antibody (sheep anti–mouse IgG, F(ab)$_2$ fragment, conjugated with 5(6)-carboxy-fluorescein-*N*-hydroxysuccinimide ester [FLUOS], no. 1214616; Boehringer Mannheim) diluted 1:15 in PBS. Tubulin immunostained slides, after two 5-min washes in PBS, were incubated for 2 h at 37°C in rhodamine-labeled phalloidin (Molecular Probes, Eugene, Oregon) dissolved in PBS (100 μl of the stock solution were vacuum dried and dissolved in 200 μl PBS). After a quick wash in PBS, slides were stained with Hoechst 33258 and mounted as described by Cenci et al. (1994).

Fluorescence Microscopy

Preparations stained with Hoechst 33258 and anti-tubulin Ab plus FLUOS-conjugated secondary Ab were examined with a Zeiss III photomicroscope equipped for epifluorescence with an HBO 100W mercury lamp (Osram). Hoechst 33258 and FLUOS fluorescence were detected using the 0.1 (BP 365/11, FT 395, LP 397) and the 0.9 (BP 450-490, FT 510, LP 420) Zeiss filter sets, respectively. Photomicrographs were recorded on Kodak T-MAX 100 film.

Preparations stained with Hoechst 33258, anti-tubulin Ab plus FLUOS-conjugated secondary Ab, and rhodamine-labeled phalloidin were examined with a Zeiss Axioplan microscope equipped for epifluorescence with an HBO 50W mercury lamp (Osram) and with a cooled charge-coupled device (Photometrics Inc., Woburn, MA). Hoechst 33258, FLUOS, and rhodamine fluorescence were detected with the 0.1, 10 (BP 450-490, FT 510, LP 515-565) and 15 (BP 546, FT 580, LP 590) Zeiss filter sets, respectively. The fluorescence signals were recorded separately as gray-scale digital images using IP Lab Spectrum software. Images were then converted to Photoshop format (Adobe Systems, Inc., Mountain View, CA), pseudocolored, and merged.

Nucleic Acids

Molecular techniques not specifically outlined here were performed using standard protocols (Sambrook et al., 1989).

Isolation of twinstar Genomic and cDNAs. 0.5 μg of total genomic DNA isolated from heterozygous *twinstar* adults was digested with Sau3A (for *tsr*^{1}) or with either EcoR1 or PstI (for *tsr*^{2}). The DNA was precipitated with ethanol, dried, and then resuspended in 400 μl of DNA ligation buffer. Circular DNA containing one end of the P element adjacent to *twinstar* genomic sequences was cloned by one of two methods. For *tsr*^{1}, the ligation was amplified with primers from the P element ends using an

inverse PCR protocol (Ochman et al., 1988). The PCR product was digested with restriction enzymes unique to the PCR primers and cloned into Bluescript KS II$^+$. For *tsr*^{2}, the ligation mix was transformed directly into XL-1 Blue cells by the $CaCl_2$ method and desired recombinants were selected with ampicillin. This "plasmid rescue" (Pirotta, 1986) was possible since the P element causing the *tsr*^{2} mutation contains a bacterial origin of replication and a selectable marker for ampicillin resistance. Wild-type genomic clones were isolated from an EMBL3 phage genomic library (kindly supplied by J. Tamkun, University of California, Santa Cruz, CA) using the PCR product described above as a probe. Restriction fragments were subcloned into Bluescript KS II$^+$. The full-length *twinstar* cDNA was isolated from a 0–4-h embryonic library (Brown and Kafatos, 1988) using genomic fragment RS6.4 (Fig. 7 *A*) as a probe.

Sequencing of Genomic and cDNAs. Sequencing of double-stranded plasmid DNA was performed by the dideoxy method (Sanger et al., 1977) using Sequenase version 2.0 (United States Biochemical Corp., Cleveland, OH) or the Ladderman kit (Takara Biochemical Inc., Berkeley, CA), ^{35}S-dATP (Amersham), 6% Long Ranger (AT Biochem, Malvern, PA) gels, and either Bluescript primers or sequence-specific primers (Biotechnology Synthesis and Analytical Facility, Cornell University, Ithaca, NY). The *twinstar* cDNA and the 6.4-kb genomic fragment used to rescue the *tsr*^{1} and *tsr*^{2} mutants (RS6.4) were completely sequenced on both strands. Sequence analysis was performed using the GCG (Devereux et al., 1984) and MacVector/AssemblyLIGN software packages (Kodak/IBI, New Haven, CT). Computer searches of GenBank and EMBL were performed using FASTA (Pearson and Lipman, 1988). The alignment of related proteins was generated with the assistance of the Clustal V program included in GCG. To obtain sequences at the 5′ end of *tsr* messages, RACE amplification of *twinstar* mRNA from wild-type (Oregon R) or mutant animals was performed on a Hybaid OmniGene thermal cycler using a GIBCO BRL kit and three nested primers specific to the *twinstar* mRNA (GIBCO BRL, Gaithersburg, MD). Primer 5′-AGTTTATTGGCGGTCGG-3′ was used for reverse transcription. The resulting first strand was PCR amplified using primer 5′-CTAGAAAACTGGTCGTAC-3′. This product was reamplified using primer 5′-TGCAGACATCAGACACAGTTACAC-3′, which was located just downstream of the first (1.5 kb) intron to ensure that final products were not due to contaminating genomic DNA. RACE products were cloned using the pCR-Script SK(+) cloning kit (Stratagene).

Northern Analysis of tsr mRNAs. Total RNA was isolated by a modification of the method of Chirgwin et al. (1979). Animals were homogenized in modified G buffer (6 M guanidine thiocyanate; 0.025 M sodium acetate, pH 7.0; 5 mM dithiothreitol) plus 0.5% *N*-lauryl sarcosinate and 0.5% diethylpyrocarbonate, then extracted once with an equal volume of a 1:1 mixture of phenol and chloroform/isoamylalcohol (24:1). After centrifugation, the aqueous layer was recovered and RNA was precipitated by adding 1/50 vol of 1 M acetic acid and 1/2 vol of ethanol. This was incubated at −20°C for 3 h, and the RNA pelleted by centrifugation in a microcentrifuge. The pellet was resuspended in one-half the original volume of G buffer, and the RNA was reprecipitated as before. Total RNA was resuspended in sterile DEPC-treated H_2O and quantitated by absorbance at 260 nm. For the developmental Northern, poly(A)$^+$ RNA was isolated using PolyA-Tract System III (Promega Corp., Madison, WI). Northern sample buffer was added to samples before electrophoresis on 1.2% agarose-formaldehyde gels as described in Sambrook et al. (1989). RNAs were then transferred to Nylon 66 (Genescreen; Schleicher & Schuell, Inc., Keene, NH) neutral membrane by electroblotting in 0.1× TAE or, for the developmental Northern, to Z Probe membrane (Bio-Rad Labs., Richmond, CA) by vacuum blotting. 300 μl of 2.5 mg/ml salmon sperm DNA was added to purified random hexanucleotide-primed probes labeled using α-[^{32}P]dCTP (Amersham) and the mixture boiled for 5 min before hybridization. Membranes were prehybridized for at least 1 h at 42°C in 50% formamide, 5× SSPE, 2× Denhardt's, and 0.1% SDS before overnight hybridization at 42°C in the same buffer. Two 45-min washes were performed at 42°C in 50% formamide, 5× SSPE, 0.5% SDS followed by two 20-min washes at 65°C in 1× SSPE, 0.5% SDS. Membranes were then exposed to Kodak X-ray film at −70°C with intensifying screens. Membranes were hybridized with a *D. melanogaster rp49* clone (O'Connell and Rosbash, 1984) as a control for loading.

Results

Identification of the twinstar Locus

We have previously described a screening procedure to identify mutations causing aberrations during mitosis (Gatti and Baker, 1989; Gatti and Goldberg, 1991). One would expect that homozygosity for mutations in many genes encoding components of the mitotic apparatus would result in lethality in late larval (third instar) or pupal stages. This is because the heterozygous mother of homozygous mutant individuals would contribute maternally supplied products to enable the earliest rounds of embryonic and larval mitosis to proceed. However, metamorphosis could not occur because the homozygous mutant zygotic genome would be unable to direct the synthesis of these molecules in imaginal discs, histoblasts, or in the larval brain. Examination of cell division in mutant larval brains would therefore reveal potential mitotic defects. This strategy has been used with considerable success to identify a variety of mitotic mutations in *Drosophila* (reviewed by Ripoll et al., 1987; Glover, 1989; Gatti and Goldberg, 1991).

We identified the mutation *twinstar*^{1} (*tsr*^{1}) by screening a collection of recessive, larval/pupal lethal mutations for mitotic abnormalities in larval brains; the mutation *twinstar*^{2} (*tsr*^{2}) was recovered in a similar manner in the laboratory of Dr. M. Fuller (Stanford University School of Medicine, Palo Alto, CA) by screening a different collection of mutations (see Materials and Methods). *tsr*^{1} and *tsr*^{2} mutants exhibit similar mitotic phenotypes (see below) and fail to complement for both lethality and cytologically detectable mitotic defects.

On the basis of several criteria, the *twinstar* gene defined by these two mutations is located near the border between polytene chromosome intervals 60A and 60B (bands 60A10-60B1). First, probes containing P element-specific sequences hybridize only to this location in *tsr*^{1} and *tsr*^{2} mutant salivary gland chromosome squashes (data not shown). Second, deficiency mapping of *tsr* mutations places the gene in the region 60A8-16 (Fig. 1). Experiments kindly performed by Dr. Bruce Reed (Whitehead Institute, Cambridge, MA) have established that the *tsr* mutations are not allelic to any of the large number of genes he has previously characterized in this interval of chromosome 2R. Thus, *twinstar* represents a new lethal complementation group in this region. Finally, both alleles have been reverted by transposase-mediated excision of the P elements (see Bellen et al., 1989; Gatti and Goldberg, 1991), demonstrating that the P element insertions in the 60A10-60B1 interval are in fact the cause of both the *tsr*^{1} and *tsr*^{2} mutations.

The Cytological Phenotype of Twinstar Mutant Neuroblasts

In larval neuroblasts of *tsr*^{1}/*tsr*^{1}, *tsr*^{2}/*tsr*^{2}, and *tsr*^{1}/*tsr*^{2} individuals, the major cytological consequence of lesions in the *twinstar* gene is the appearance of a significant proportion of polyploid cells (Fig. 2; Table I). Other aspects of mitosis appear to be largely unaffected. The mitotic index, a parameter measuring the frequency of cells engaged in mitosis, is nearly normal (Table I). The percentages of mitotic cells that are in anaphase in mutants are very similar to wild-type. Chromosomes in mutant neuroblasts seem to be normal: we see no evidence of irregular chromosome condensation or of chromosome breakage (Gatti and Baker, 1989).

The phenotype observed in both *tsr*^{1} and *tsr*^{2} brains is similar to that associated with mutations in a variety of

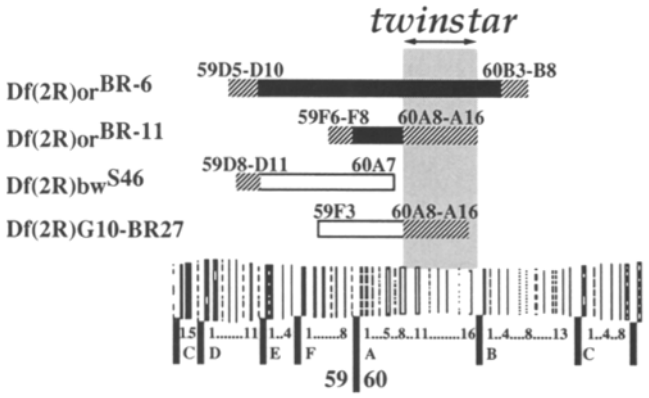

Figure 1. Deficiency mapping of the *twinstar* locus. *twinstar* fails to complement $Df(2R)or^{BR\text{-}6}$ (59D5-10;60B3-8) and $Df(2R)or^{BR\text{-}11}$ (59F6-8;60A8-16) (*filled bars*), but does complement $Df(2R)bw^{S46}$ (59D8-11;60A7) and *Df(2R)G10-BR-27* (59F3;60A8-16) (*open bars*). Stretches of DNA that are absent in deficiency strains are represented by solid bars, with uncertainties in deficiency breakpoint ends indicated by crosshatching; the *twinstar* locus is thus contained within the shaded region (60A8-16). The right-hand breakpoint of $Df(2R)or^{BR\text{-}11}$ is shown to be distal to that of *Df(2R)G10-BR-27* based on genetic mapping against other complementation groups in this region (Dr. Bruce Reed, personal communication). Probes containing sequences found within the P element transposons also hybridize to the region 60A10-60B1 in squashes of salivary gland chromosomes (not shown).

genes that cause defects in cytokinesis (Gatti and Baker, 1989; Karess et al., 1991; Castrillon and Wasserman, 1994; Neufeld and Rubin, 1994). Successive failures in cytokinesis would result in cells that increase their ploidy geometrically, giving rise to large polyploid cells such as that shown in Fig. 2 *d*. The normality of other mitotic parameters suggests that these lesions in the *twinstar* gene do not significantly alter other mitotic processes. An example of this specificity is shown in Fig. 2 *e*, which demonstrates that polyploid cells, which must already be depleted for normal tsr^+ function, are nonetheless able to enter anaphase. Fig. 2 *f* shows an anaphase spindle that is multipolar due to the retention of several centrosomes in a single cell, another expected result of failures in cytokinesis.

Meiotic Aberrations Associated with Mutations in twinstar

Male meiosis offers a particularly suitable system for the analysis of the cytological consequences of mutations affecting cell division. Primary spermatocyte nuclei are ~25 times larger than neuroblast nuclei and exhibit comparatively larger spindles that can be clearly detected by tubulin immunostaining. We have recently provided a detailed description of chromosome and microtubule organization during wild-type male meiosis, which we have been able to subdivide into cytologically well-defined stages (Cenci et al., 1994). Because meiosis occurs in the testes of third in-

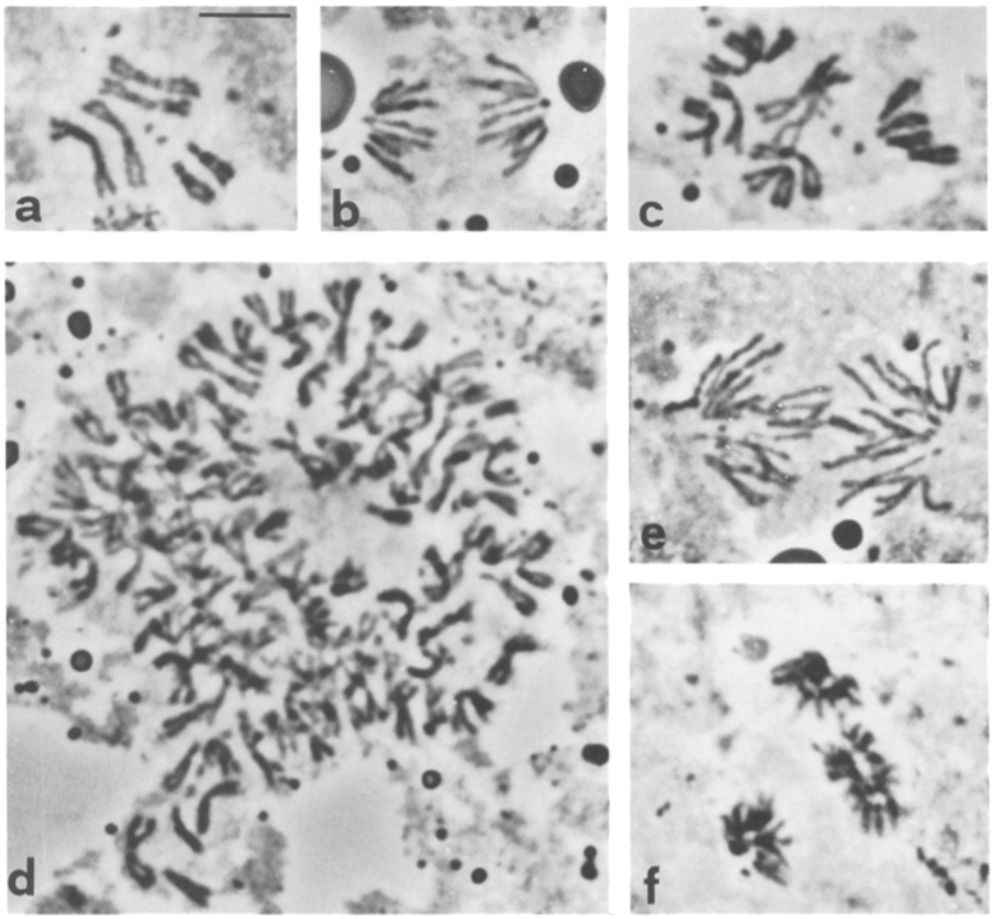

Figure 2. Mitotic defects in larval neuroblasts of *tsr* mutants. (*a*) Diploid female metaphase and (*b*) diploid anaphase from Oregon R controls. (*c*) Tetraploid metaphase, (*d*) highly polyploid metaphase, (*e*) tetraploid anaphase, and (*f*) tripolar polyploid anaphase from tsr^1/tsr^1 larval brains. Bar, 5 μm.

Table I. Frequency of Polyploid Cells and Mitotic Parameters in Larval Neuroblasts of tsr Mutants

Genotype	No. of brains	No. of metaphases		No. of anaphases		No. of cells scored	% polyploid figures	% anaphases	Mitotic index*
		diploid	polyploid	diploid	polyploid				
tsr^1/tsr^1	23	1190	211	233	10	1644	13.4	14.8	0.78
tsr^2/tsr^2	10	937	108	232	3	1280	8.7	18.4	0.92
tsr^1/tsr^2	9	519	128	117	9	773	17.7	16.3	0.84
Oregon R	5	478	0	94	0	572	0.0	16.4	0.71

*Mitotic figures were scored every fourth optic field in each brain examined (see Materials and Methods).

star larvae, we were able to analyze the meiotic divisions in mutant *tsr* larvae for potential aberrations.

Improper Aster Migration during Prophase/Prometaphase of Both Meiotic Divisions. A unique phenotypic consequence of lesions in *twinstar* occurs in primary spermatocytes at the prophase/prometaphase transition of meiosis I, and is revealed when fixed mutant testes are stained with antibodies directed against tubulin. In wild-type males, centrosomes reside just under the plasma membrane throughout most of the primary spermatocyte stage (see Fig. 10 below), during which growth and gene expression prepare the cell for subsequent morphological differentiation (Tates, 1971; reviewed by Fuller, 1993). Near the end of this spermatocyte maturation phase, duplicated centrosomes (each containing a pair of centrioles) migrate together to the nuclear membrane, where they nucleate prominent asters (Tates, 1971; Cenci, 1994; see also Fig. 9 *c* below). During late prophase/early prometaphase of the first meiotic division (stage M1a), the two asters separate from each other and migrate around the periphery of the nuclear envelope, in preparation for the establishment of the bipolar spindle. By early prometaphase, asters are located directly opposite each other on either side of the nucleus, in close apposition to the nuclear membrane. Wild-type spermatocytes at the M1a stage are shown in Fig. 3 *a*.

In *tsr* spermatocytes at the M1a stage, the two asters often remain in close proximity to each other and fail to associate with the nuclear envelope (Fig. 3 *b*). We have named the *twinstar* gene after this characteristic aberrant arrangement of asters. This effect occurs in a very high proportion of *tsr* primary spermatocytes, approaching 100% in tsr^1 mutants (Table II), but is almost never seen in wild-type. Somewhat later, in the M1b stage, asters in *tsr* mutants can be seen to separate slightly (Fig. 3 *c*), but remain unassociated with the nuclear membrane.

It is remarkable that subsequent to the M1 stage, the spindles in *tsr* mutant spermatocytes progressively resume a relatively normal position and appearance and seem indistinguishable from wild-type throughout the remainder of the first meiotic division (Fig. 4). However, after com-

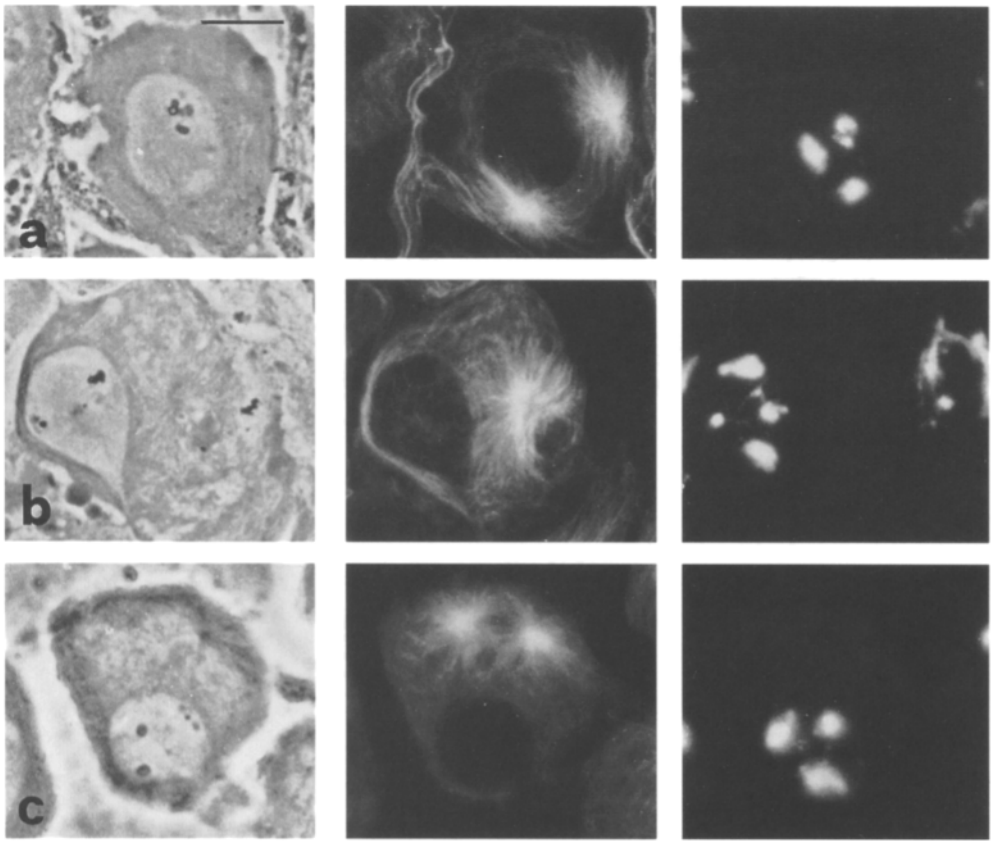

Figure 3. Aster migration in meiotic prometaphase I of tsr^1/tsr^1 males. (*Left*) Phase contrast; (*middle*) anti-tubulin staining; (*right*) Hoechst 33258 staining of DNA. (*a*) A primary spermatocyte in the M1a stage from Oregon R controls, showing well separated asters closely apposed to the nuclear envelope. (*b* and *c*) Primary spermatocytes in (*b*) M1a and (*c*) M1b stages from tsr^1/tsr^1 males. Note the delay in migration and abnormal positioning of asters with respect to the cell nucleus. Stage identification was based on the presence of intranuclear granules originating from Y loop disintegration and on the relative size of spermatocyte nuclei (for details see Cenci et al., 1994). Bar, 10 μm.

Table II. Meiotic Abnormalities in tsr Mutants

	Asters in prometaphase I			Asters in prometaphase II			Spermatids‡			
Genotype	Normal	Irregular*	% Irregular	Normal	Irregular*	% Irregular	1:1	2:1	3:1 and 4:1	% Irregular
tsr1/tsr1	2	117	98.3	34	91	72.8	422	108	73	30.0
tsr2/tsr2	12	104	89.6	31	56	64.3	602	23	5	4.4
Oregon R	99	2	2.0	98	2	2.0	200	0	0	0.0

*Irregular positioning and/or delayed migration of asters.
‡Ratios refer to number of nuclei per Nebenkern. 1:1, regular spermatids containing one nucleus and one Nebenkern of similar size.
Failures in cytokinesis are revealed by other patterns (see text): 2:1, two nuclei associated with one large Nebenkern. 3:1 and 4:1, three or four nuclei associated with one large Nebenkern.

pletion of meiosis I, *tsr* prophase/prometaphase secondary spermatocytes (stage M6a and M6b) exhibit the same defect in aster migration and positioning observed in primary spermatocytes (Fig. 5). Here again, the spindles become more normal by metaphase II and retain a wild-type structure throughout the remainder of meiosis II. Although telophase II *tsr* spindle structures look normal, we often observed an aberrant cross-like configuration of meiotic spindles that overlap at the midbody (Fig. 5 *j*). Most likely this arrangement reflects a failure of the first meiotic cytokinesis and the consequent occurrence of two second divisions within the same cell (see below).

The analysis of hundreds of ana-telophases of *tsr* mutants showed no evidence of irregular chromosome segregation during either meiotic division. We never observed lagging chromosomes or daughter nuclei of different size. In addition, *tsr* "onion stage" spermatids exhibit a uniform nuclear size (see below). As it has been demonstrated that spermatid nuclear size is proportional to chromosome content (González et al., 1989), this observation reinforces the conclusion that *tsr* does not affect chromosome segregation.

Failure of Cytokinesis during Spermatogenesis in twinstar Larvae. During both meiotic divisions in wild-type spermatocytes, mitochondria associate lengthwise along the spindle apparatus (see Figs. 4 and 5; Cenci et al., 1994), which is pinched in half during cytokinesis, ensuring an even distribution of these organelles to each of the two daughter cells. Immediately after completion of meiosis, the mitochondria associated with each hemispindle fuse and form an interlaced conglomerate called the Nebenkern. Thus, each newly formed wild-type spermatid (referred to as the onion stage) consists of a round, phase-light nucleus associated with a single phase-dark Nebenkern of similar size (Fig. 5 *o*; reviewed by Fuller, 1993).

The most obvious defect in *tsr* mutants is seen in spermatids at the onion stage. In *tsr* mutant testes, a substantial fraction of onion stage spermatids contain a single Nebenkern much larger than normal, along with four normal-sized nuclei (Fig. 5 *q*; Table II). This phenotype re-

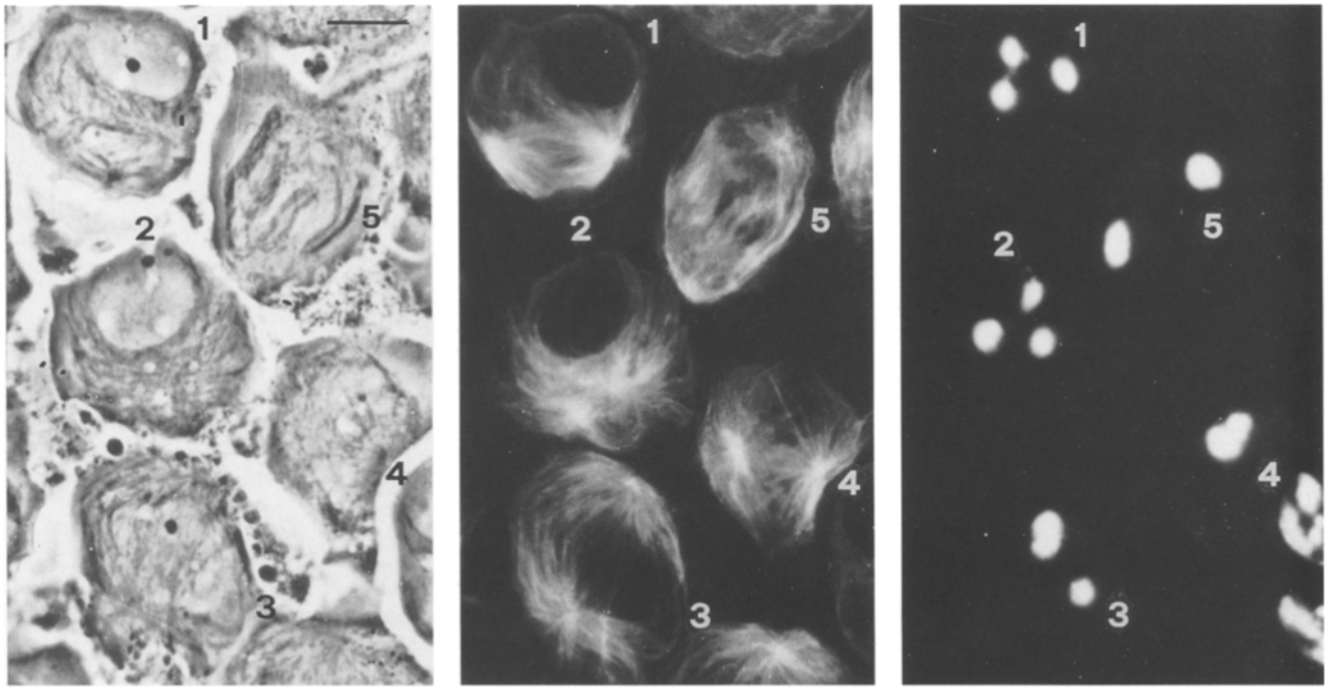

Figure 4. First meiotic division in *tsr* mutants. The three panels show the same partial cyst containing primary spermatocytes at different meiotic stages. (*Left*) Phase contrast; (*middle*) anti-tubulin staining; (*right*) Hoechst 33258 staining of DNA. 1 and 2, spermatocytes in early meiotic prometaphase (M1b stage) showing delayed migration and abnormal positioning of asters. 3, prometaphase (stage M2), and 4, metaphase (stage M3) spermatocytes in which the asters have almost attained a regular bipolar arrangement. 5, a morphologically normal mid-anaphase (stage M6b). Bar, 10 μm.

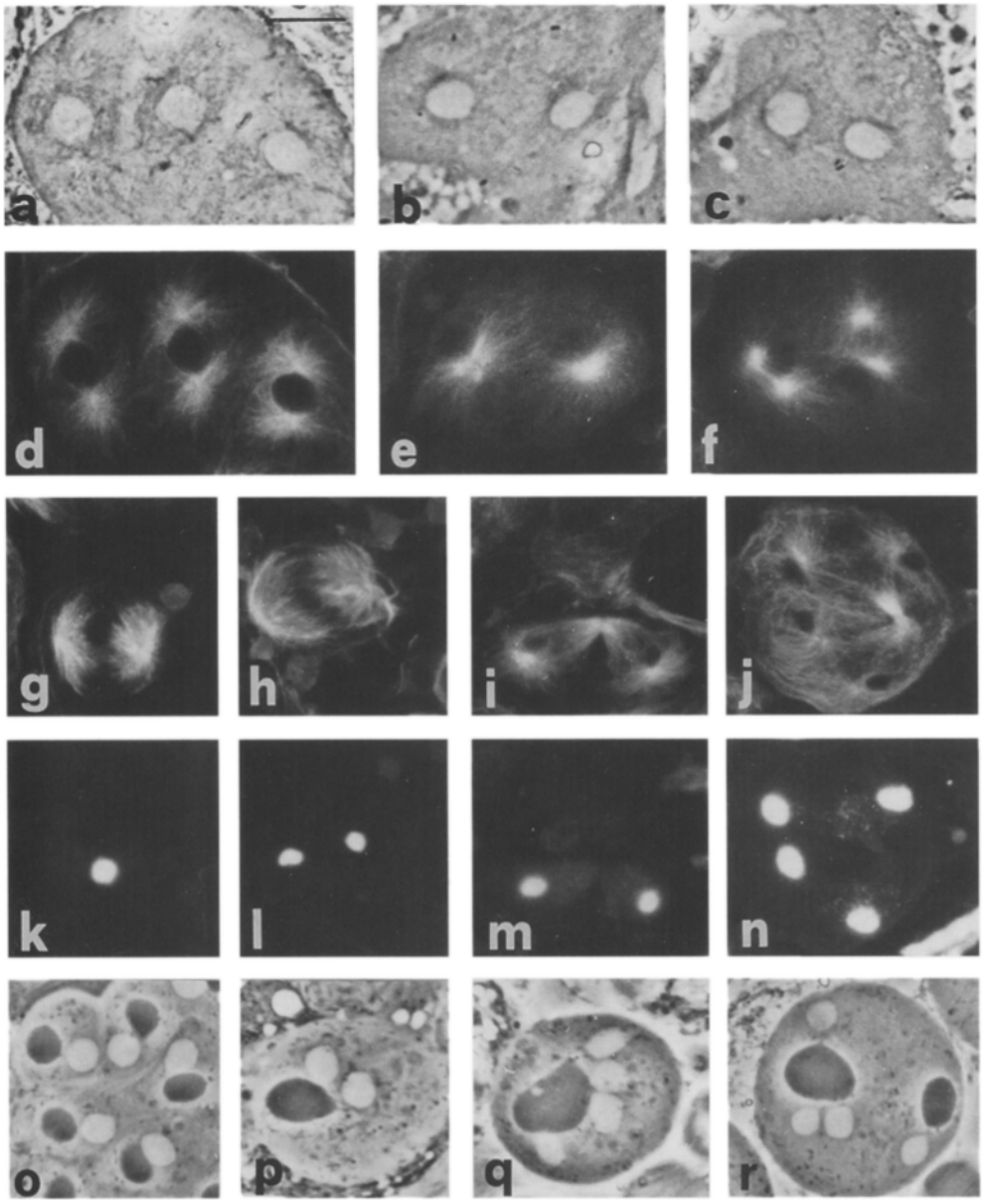

Figure 5. Second meiotic division and postmeiotic stages in *tsr* mutants. *a–f* show partial secondary spermatocyte cysts observed by phase contrast microscopy (*a–c*) and after immunostaining with anti-tubulin Abs (*d–f*). (*a* and *d*) Prometaphase II (stage M7) spermatocytes from Oregon R controls with normally positioned asters. (*b* and *e*, *c* and *f*) The same stage from tsr^1/tsr^1 males showing delayed migration and abnormal positioning of asters. *g–n* show meiotic cells immunostained with anti-tubulin Abs (*g–j*) or stained with Hoechst 33258 (*k–n*). (*g* and *k*) A metaphase cell in the M9 stage in which the asters have almost attained a regular bipolar arrangement. (*h* and *l*) An early anaphase (stage M10a), and (*i* and *m*) an early telophase (stage M11), both with regular spindles. (*j* and *n*) Two late telophase II occurring in the same cytoplasm, showing overlapped central spindles. *o–r* show living spermatids at the onion stage observed with phase contrast. (*o*) Regular spermatids from Oregon R controls with nuclei (*white discs*) and Nebenkerns (*dark discs*) of similar sizes. (*p–r*) Spermatids from *tsr* mutants showing large Nebenkerns associated with (*p*) two, (*q*) four, or (*r*) three nuclei. See text for details on the origin of these aberrant spermatids. Bar, 10 μm.

flects a failure of cytokinesis at both meiosis I and II, as this would prevent proper subdivision of the mitochondrial complement into four Nebenkerns (reviewed by Fuller, 1993). We also see cells with two normal-sized nuclei in association with an intermediate-size Nebenkern (Fig. 5 *p*; Table II), indicating a failure of cytokinesis at only one of the meiotic divisions. Because failure of cytokinesis in the first meiotic division would lead to cells containing two second division meiotic spindles (see Fig. 5, *j* and *n*) that would probably encounter further difficulties in cytokinesis, we believe that the spermatids with one Nebenkern and two nuclei are the result of second division cytokinesis failure. Finally, we observe spermatids containing one large Nebenkern plus three nuclei that are usually located in close proximity to a cell containing a normal-size Nebenkern and a single regular nucleus (Fig. 5 *r*; Table II). These are most likely to arise if the four hemispindles in secondary spermatocytes derived from cytokinesis I failures (see again Fig. 5, *j* and *n*) orient in such a way that mitochondrial fusion occurs asymmetrically, yielding a small and a large Nebenkern associated with one and three nuclei, respectively.

Molecular Analysis of the twinstar Gene

Molecular Cloning and Transcriptional Analysis of twinstar. A small stretch of DNA adjacent to the P element insertion in tsr^1 was initially cloned using an inverse PCR protocol and then used to screen a wild-type *Drosophila* genomic library. A 6.4-kb EcoR1-SalI subclone from this library (RS6.4) surrounds the tsr^1 and tsr^2 P element insertion sites (Fig. 6 *A*). Whole genome Southern analysis confirmed the presence of P element insertions within this fragment in both *tsr* mutant alleles that were absent from

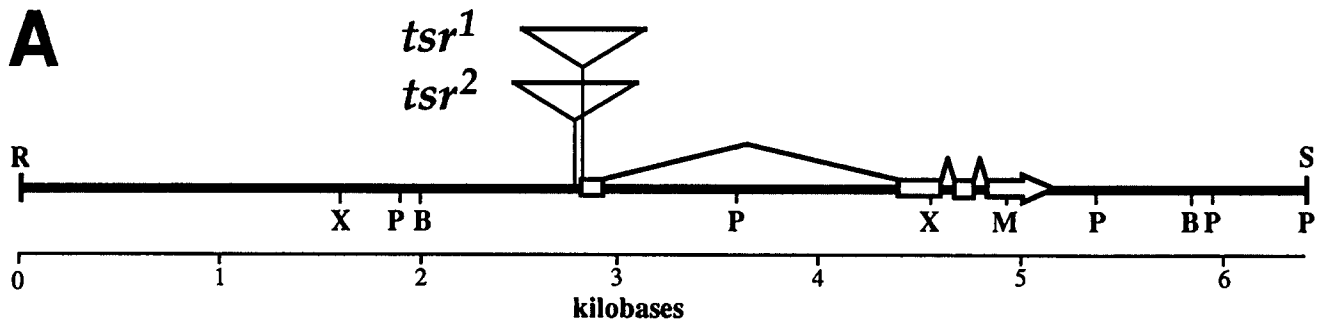

B

▼tsr 2 ▼tsr 1

```
2701  aacgtcgcgacgcgtcacgacgcatgttgatactttgccggcgcctggcaaccctaacctgtgcgaaataaccgaccaaattgattcgtcoggttgttcg
2801  tgaaagaaggcggaaggttaaacagtatttgtaaaatatatactoggcgaagcagcaatttgagaattgtgaaagcgaaaaactacaggaaaaATGgtac
                                                                                          M
....
4301  cttggttgacagtttggcgcgcattgaacattcaaaatacattctctgatttgcatctctaccttctctctctctaaagGCTTCTGGTGTAACTGTGTCT
                                                                                    A  S  G  V  T  V  S
4401  GATGTCTGCAAGACTACATACGAGGAAATAAAGAAGGACAAAAAGCATCGCTATGTCATCTTTTACATTCGCGATGAAAAGCAGATTGATGTGGAGACTG
       D  V  C  K  T  T  Y  E  E  I  K  K  D  K  K  H  R  Y  V  I  F  Y  I  R  D  E  K  Q  I  D  V  E  T
4501  TGGCAGATCGCAACGCCGAGTACGACCAGTTTCTAGAAGATATCCAGAAATGCGGACCTGGAGAGTGCCGgtaagttccgccggttagagacacccagac
      V  A  D  R  N  A  E  Y  D  Q  F  L  E  D  I  Q  K  C  G  P  G  E  C  R
4601  ccatcgaaactaacctaatttaacatctattcgcttgcacagGTACGGACTGTTCGATTTCGAGTACATGCACCAGTGTCAAGGCACCTCTGAGAGTTCA
                                                Y  G  L  F  D  F  E  Y  M  H  Q  C  Q  G  T  S  E  S  S
4701  AAGAAGCAAAAGCTGTTCCTTATGTCGTGGTGTCCCGATACTGCCAAGgtatgtgaatagccagttgccaagtaatggcgcagaactcatttcgatatca
       K  K  Q  K  L  F  L  M  S  W  C  P  D  T  A  K
4801  cacacccacagGTCAAGAAGAAGATGTTGTACTCCAGCTCCTTCGATGCTCTCAAGAAGTCGCTCGTGGGCGTCCAAAAGTATATACAAGCCACTGATCT
                  V  K  K  K  M  L  Y  S  S  S  F  D  A  L  K  K  S  L  V  G  V  Q  K  Y  I  Q  A  T  D  L
4901  TTCCGAAGCCTCCCGGGAAGCCGTCGAGGAGAAACTCCGGGCCACCGACCGCCAAtaaactgtacgagcactgtgcattgcatttaacaaacaaggcatg
        S  E  A  S  R  E  A  V  E  E  K  L  R  A  T  D  R  Q
5001  catgaaacagcgatggaaacaogtatcctgttgagatcgccaatttgtatgagaattttctacataatttgtattttcagtagaaataaagaatgaaata
5101  tttaacttgaccaagtcgcgtttccgctgtggtaaaaatctcgtaccgcagaatacactttattataaggagcaaagattacattgtacatatgatgacg
```

Figure 6. Molecular analysis of *twinstar*. (*A*) Physical map of the *twinstar* genomic region. The 6.4-kb genomic fragment used to rescue the *twinstar* mutants (RS6.4) is shown. Approximate positions of the P elements causing the tsr^1 and tsr^2 alleles are indicated. The *twinstar* cDNA (open boxes and arrow), when mapped onto the genomic fragment, is interrupted by one large (1.5 kb) and two small (72 and 63 bp) introns. The direction of transcription is from left to right in this diagram; we do not know the transcriptional polarity relative to the chromosome as a whole. Restriction sites shown: EcoR1 (*R*), XhoI (*X*), BamH1 (*B*), PstI (*P*), SmaI (*M*), SalI (*S*). (*B*) Excerpts from the DNA sequence of RS6.4, showing regions containing the P element insertion sites and the *twinstar* cDNA sequence. Arrowheads mark insertion sites of the P elements causing the tsr^1 and tsr^2 alleles. These are located 19 bp apart: the tsr^1 insertion site occurs 5 bp within the 5′UTR of the cDNA, while that of tsr^2 lies just upstream. cDNA sequence is in boldface type; coding regions are in capitals, with one letter amino acid codes centered beneath each codon. Genomic sequences not present in the cDNA are italicized. The cDNA carries one noncoding G at the 5′ end (not pictured). The putative polyA addition signal sequence is underlined. Since the sequence shown corresponds to part of the sequence from the 6.4 kb of RS6.4, this figure uses a nucleotide numbering scheme that is relative to the entire fragment. Genbank accession numbers: *twinstar* cDNA, U24490; genomic fragment RS6.4, U24676.

wild-type DNA and from DNA of transposase-induced revertants of both alleles (data not shown). Probes made from RS6.4 hybridized in situ to polytene chromosome interval 60A10-60B1, in good agreement with the cytogenetic position of *twinstar*.

Based on Northern analysis suggesting that RS6.4 hybridizes to a single species of poly(A)$^+$ RNA 800-900 bp in length (see below), we reintroduced genomic fragment RS6.4 into the *Drosophila* genome via P element-mediated germline transformation. A single transduced copy of RS6.4 corrects the lethality as well as the mitotic and meiotic phenotypes associated with mutant alleles of *tsr*. Thus, tsr^+ genetic activity is contained within the 6.4 kb of genomic fragment RS6.4.

The level of the single transcript detected by RS6.4 is decreased in homozygous tsr^1 and tsr^2 mutants to no more than 20% of wild-type and is restored to wild-type levels in rescued lines (Fig. 7 *A*). This transcript is expressed during all stages of *Drosophila* development, is found in both adult males and females, and appears to peak in late larval and pupal stages (Fig. 7 *B*). On the basis of these and other data (see below), we believe that this cDNA represents the *twinstar* transcript.

We have determined the entire nucleotide sequence of RS6.4 and that of an homologous 750-bp cDNA clone (Fig. 6 *B*). The putative *tsr* cDNA insert contains a single long, ATG-initiated open reading frame. The nucleotide sequence flanking this putative translational start, AAAAATG, is consistent with the *Drosophila* translation initiation consensus (C/A)AA(A/C)ATG (Cavener, 1987). A consensus signal sequence for polyA addition is located 25 bases upstream from the polyA stretch found in the cDNA. Comparison of the genomic and cDNA sequences indicates that the *twinstar* gene is interrupted by one long (1.5 kb) and two small (72 bp and 63 bp) introns (Fig. 6), which are flanked by consensus splice donor and acceptor sites

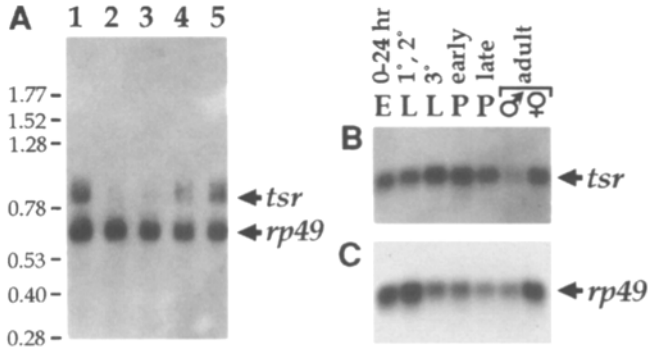

Figure 7. Northern analysis of *twinstar* mRNA. (*A*) Expression of *twinstar* in mutant and rescued lines. Lane *1*, wild type (Oregon R); lane *2*, tsr^1/tsr^1; lane *3*, tsr^2/tsr^2; lane *4*, tsr^1/tsr^1;[pW8-tsr^+]/[pW8-tsr^+]; lane *5*, tsr^2/tsr^2;[pW8-tsr^+]/[pW8-tsr^+]. Lanes *2* and *3* are *tsr* mutant strains; lanes *4* and *5* are the same *tsr* mutant lines that have been rescued with wild-type genomic DNA spanning the *tsr* locus (see text). On this blot, *tsr* expression in the mutants appears negligible, but we estimate from additional experiments that mutants may contain a residual level of *tsr* mRNA up to 20% of wild-type. 10 μg of total RNA isolated from third instar larvae were loaded in each lane. RNA molecular weight standards (in kb) are indicated at left. (*B*) Developmental expression of *twinstar* in wild-type animals raised at 25°C. Lanes: 0–24 h embryos; first and second instar larvae; third instar larvae; early pupae; late pupae; adult males; adult females. 5 μg of polyA$^+$-selected RNA were loaded in each lane. (*C*) The same blot as in *B* hybridized with *rp49* cDNA as a loading control.

(Mount, 1982). The cDNA carries one additional non-transcribed G at the 5′ end, which is thought to represent reverse transcription of the 5-methyl-G cap during cDNA synthesis (Brown et al., 1989; Ketchum et al., 1990; Karess et al., 1991; Rose and Weischaus, 1992). No other significant open reading frames were found in RS6.4, in correspondence with its hybridization to only a single RNA species on Northern blots.

By direct sequencing of mutant DNA, we determined the precise locations of the P element insertions causing the tsr^1 and tsr^2 mutations to be 19 bp apart, in or very near the beginning of the *tsr* transcript (Fig. 6 *B*). The longest product produced by RACE (rapid amplification of cDNA ends) using RNA isolated from wild-type embryos or third instar larvae extends five bases beyond the cDNA 5′ end (data not shown). This places the tsr^1 insertion site within the mRNA 5′-untranslated region (5′-UTR) and suggests that the tsr^2 insertion point would appear to be a few nucleotides upstream of the start of *twinstar* transcription. However, we do not know precisely where *tsr* mRNA transcription is initiated, nor do we see an obvious TATA box.

To investigate how detectable (though reduced) amounts of normal-sized *tsr* mRNA could be produced in mutant animals when at least one of the P element insertion sites appears to be located within the transcribed region, we also analyzed RACE products from homozygous tsr^1 and tsr^2 larvae. These products contain short (78-126 bp) unique sequences at their 5′ ends that appear to be spliced into the normal *tsr* message either at or just downstream of the P element insertion sites (data not shown). We have not been able to identify the unique 5′ regions either in the 2 kb of genomic DNA we have sequenced upstream of the insertion sites or in known sequences from the marked P elements; however, we believe they are likely to be derived from within the P elements. Decreased initiation efficiency or stability of these hybrid transcripts could then account for the low levels of *tsr*-homologous mRNAs observed in the mutants.

Twinstar Encodes a Member of the Cofilin/ADF Family of Actin Associated Proteins. Conceptual translation of the open reading frame in the *twinstar* cDNA (Figs. 6 *B* and 8) generates a 17-kD polypeptide related to proteins in the cofilin/ADF family. These proteins can sever filamentous actin and also bind and sequester actin monomers, leading to depolymerization of actin filaments (reviewed by Sun et al., 1995). A cDNA coding for the twinstar protein has also been recovered independently from a screen of a *Drosophila* cDNA library for proteins that produce changes in cell shape when overexpressed in the fission yeast *S. pombe* (Edwards et al., 1994).

An alignment of the predicted twinstar protein with representative homologues from nematode, yeast, amoeba, plant, and vertebrate (human) species is shown in Fig. 8. The four nonvertebrate sequences shown returned the highest scores in searches of the GenBank and EMBL databases, with amino acid identities in the range of 36–39% over the length of the protein when compared with twinstar. Fig. 8 highlights three regions implied in specific functions. Two conserved motifs found in proteins of the cofilin/ADF family appear to be important for actin binding based on studies with mammalian homologues, corresponding to twinstar residues 94–105 (*shaded bar*) and 112–118 (*filled bar*). These regions are implicated additionally in either phosphoinositide binding (*shaded bar* only) or competition with tropomyosin for binding to actin (*filled bar* only). A third motif present in vertebrate homologues, PXXXKKRKK (*hatched bar*), is conserved relatively well in twinstar but not in homologues from other organisms. This sequence resembles the nuclear localization signal sequence of SV-40 large T antigen, and is thought to play a role in translocation of cofilins into the nucleus under conditions of stress (see Discussion).

Actin Behavior in tsr Mutants

The finding that *twinstar* encodes a *Drosophila* cofilin homologue prompted us to compare actin behavior in *tsr* mutant and wild-type testes (Figs. 9–11). We consider first F-actin distribution within primary spermatocytes through early anaphase of the first meiotic division. In cysts of young wild-type spermatocytes (stage S1), actin forms a ribbon-like pattern that connects adjacent cells (Fig. 9 *a*); we believe this corresponds to an analog of the fusome, a structure that extends through the ring canals of developing oocytes (Lin et al., 1994). These ribbons gradually disassemble, so that in mature primary spermatocytes (stage S5), actin is only found in a loose network of cables and spots (Fig. 9, *b* and *c*). Little or no F-actin staining is visible by the time wild-type primary spermatocytes enter prometaphase (stage M1; Fig. 9 *c*; see also Fig. 11 *a*) or later through early anaphase of the first meiotic division (to stage M4b; Fig. 11 *b* and data not shown). Testes from *twinstar* mutants exhibit an actin staining pattern that is similar to that of wild-type through the mature primary spermatocyte stage (stage S5;

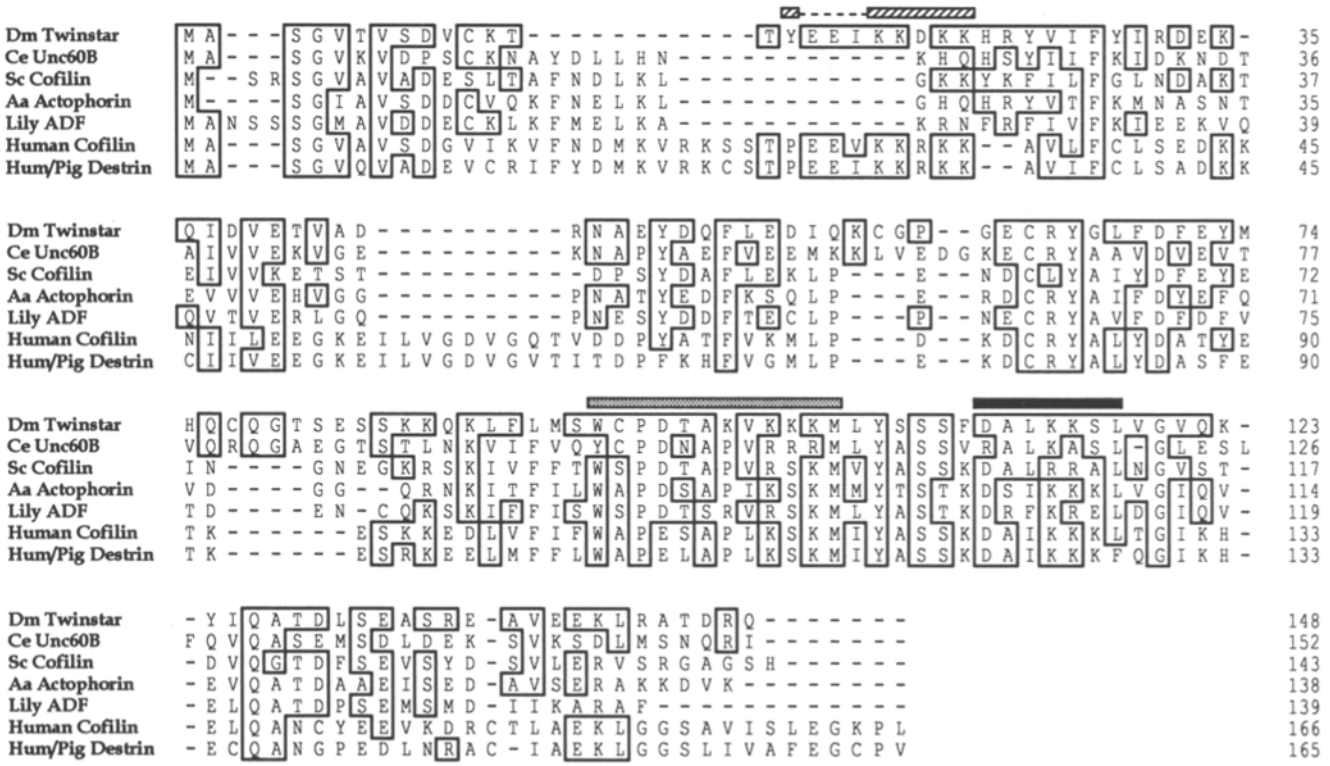

Figure 8. Comparison of the putative twinstar protein with members of the same family of small actin-severing proteins from other organisms. Sequences shown, from top down: *D. melanogaster* twinstar, *C. elegans* Unc60B (McKim et al., 1994), *S. cerevisiae* COF1 (Iida et al., 1993; Moon et al., 1993), *A. castellanii* actophorin (Quirk et al., 1993), *L. longiflorum* ADF (Kim et al., 1993), human cofilin (Ogawa et al., 1990), human and porcine destrin (Moriyama et al., 1990*b*; Hawkins et al., 1993). Overline bars indicate putative functional domains. The region defined by the shaded bar has been implicated in actin binding based on mutational (Moriyama et al., 1992), cross-linking (Yonezawa et al., 1991*a*), and peptide inhibition studies (Yonezawa et al., 1991*b*). This region also interacts with certain phosphoinositides (Moriyama et al., 1992; Yonezawa, et al., 1991*b*). The vertebrate sequence in the region indicated by the filled bar, DAIKKK, is identical to residues 2–7 at the NH_2 terminus of tropomyosin (Cho et al., 1990) and can compete with it for binding to actin (Yonezawa et al., 1989). The hatched bar represents a putative nuclear localization signal sequence present in vertebrate homologues that is similar to that of SV40 large T antigen (Matsuzaki et al., 1988).

Fig. 10 *a* and data not shown). Immediately afterwards, however, the distribution of actin in *twinstar* mutants becomes dramatically different from that in wild-type: at the S6 stage (a rapid phase of transition between the end of spermatocyte growth and the onset of meiosis), mutant primary spermatocytes develop a single large F-actin aggregate in the cytoplasm of each cell (Fig. 10, *a* and *c*). This actin cluster (which we term a type 1 aggregate) rapidly forms near the centrosomes at the cell cortex, just at the time they first begin to nucleate microtubules (Fig. 10, *b* and *c*). This aggregate remains in the vicinity of the asters when they assume their ectopic position in mutant primary spermatocytes at prometaphase (stage M1; Fig. 10 *a*; see also Fig. 11 *e*). The fact that little or no F-actin staining is seen in primary spermatocytes at the S5 stage immediately before the formation of type 1 aggregates indicates that this type of actin cluster is not simply a remnant of a previously formed actin structure in these mutant cells. At metaphase (stage M3), the actin cluster in *twinstar* mutant primary spermatocytes dissociates from the asters and is usually seen at the equator of the cell (Fig. 11 *f*). During early anaphase, type 1 aggregates essentially disappear (data not shown).

Additional differences in actin behavior become apparent by late anaphase/early telophase (stages M4c-M5). In wild-type, actin becomes concentrated at the spindle midzone where it forms a ring-like structure that contracts as the cell progresses toward telophase (Fig. 11, *c* and *d*). In *twinstar* mutants, actin also concentrates at the mid-zone of the central spindle at this time (Fig. 11 *g*). This actin focus (a type 2 aggregate) is more prominent than the wild-type contractile ring and exhibits unusual protuberances generally oriented along the central spindle axis. Type 2 aggregates are also more stable than normal contractile rings. Contractile rings in wild-type disassemble at the end of the first meiotic division (stage M5/M6), and wild-type secondary spermatocytes do not exhibit prominent actin structures from interphase to mid-anaphase (stages M6-M10b; data not shown). In contrast, type 2 aggregates persist until metaphase II (stage M9), often even increasing in size. Sometimes, a type 2 aggregate is found associated with the metaphase II spindle in only one of the two daughter cells produced by the first meiotic division (Fig. 11 *h*), but is more often found associated with the spindles in both daughter cells (Fig. 11 *i*). As the second meiotic division proceeds into anaphase II, type 2 aggregates eventually disassemble (not shown).

A final difference between actin behavior in wild-type

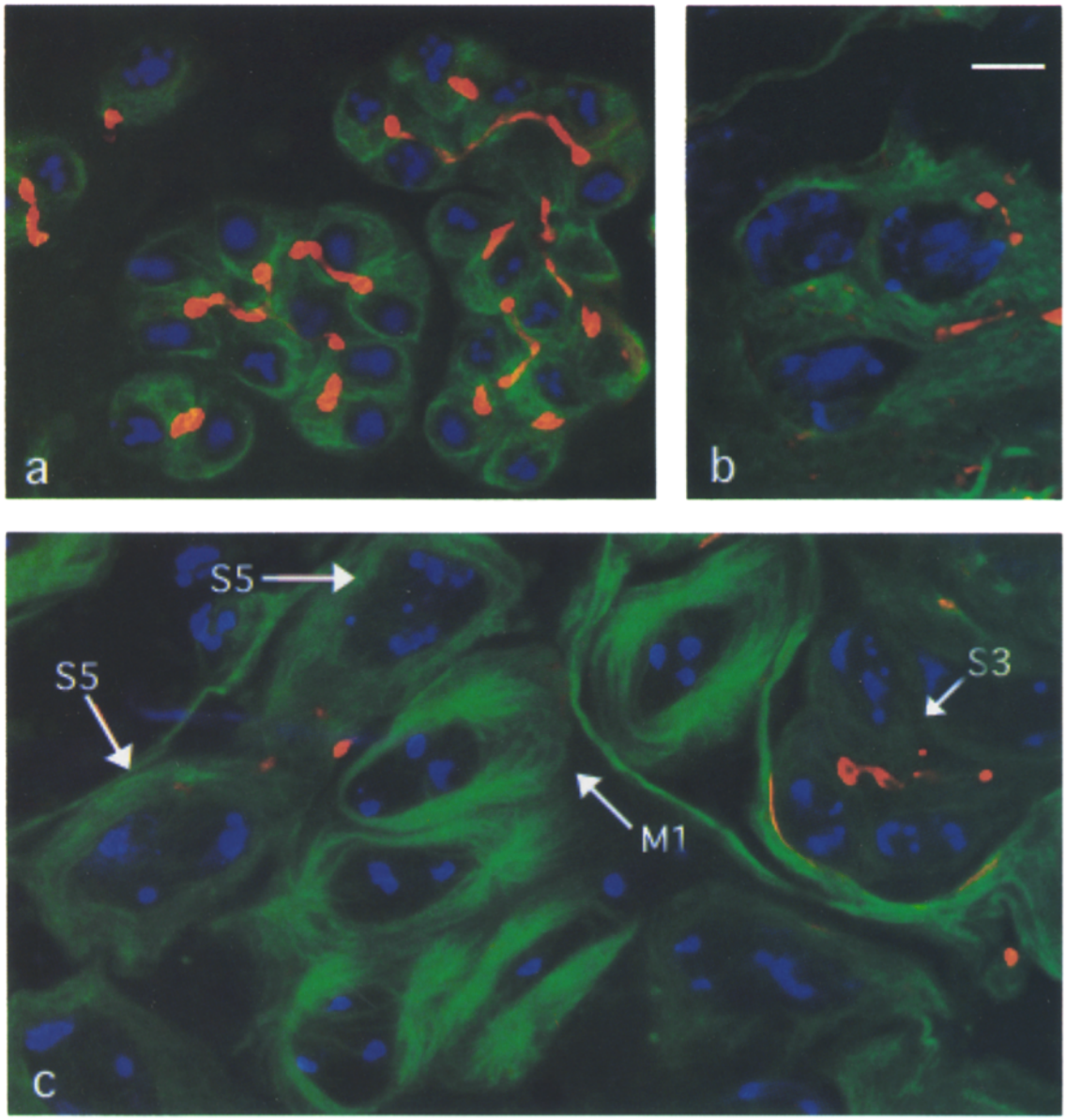

Figure 9. Actin behavior in Oregon-R wild-type primary spermatocytes through prometaphase (stages S1 to M1). To visualize tubulin, actin and DNA, testes were immunostained with anti-tubulin Abs (*green*) and then sequentially stained with rhodamine-labeled phalloidin (*red*) and Hoechst 33258 (*blue*). The fluorescent signals were detected separately by a cooled charge-coupled camera and merged in pseudocolors. Yellow and orange colors indicate overlap of actin and microtubule signals. (*a*) Partial cyst containing S1/S2 young primary spermatocytes. F-actin staining of structures connecting adjacent cells is apparent; we suggest these structures are fusome analogs (see text). (*b*) Near mature primary spermatocytes (stage S4) showing actin spots and cables. (*c*) Spermatocytes at stages S3, S5, and M1. Note that phalloidin staining gradually disappears during these stages of development, and is absent in wild-type M1 cells. Bar, 10 μm.

and mutant meiosis becomes apparent by late anaphase and telophase of the second meiotic division (stages M10c-M11). In wild-type, F-actin is localized in a clearly visible contractile ring that disappears after completion of the second meiotic division (data not shown). At the corresponding stages in *twinstar* mutants, an F-actin containing structure (type 3 aggregate) assembles at the spindle midzone. This type 3 aggregate, like the type 2 aggregate, is more prominent than the wild-type contractile ring and has protuberances oriented along the spindle axis (Fig. 11 *j*). Moreover, the type 3 aggregate does not disappear at the end of the second meiotic division, but persists until the onion stage, disassembling only during spermatid elongation (not shown).

We analyzed actin behavior in both tsr^1 and tsr^2 mutant testes, and in both cases we observed the pattern described above. The only detectable differences between the two mutant alleles are in the size and morphology of the aberrant actin aggregates. The type 1 aggregate of tsr^2 is somewhat smaller than that of tsr^1. Similarly, the type 2 and type 3 aggregates of tsr^2 tend to be less prominent and are more regular in shape than those observed in tsr^1.

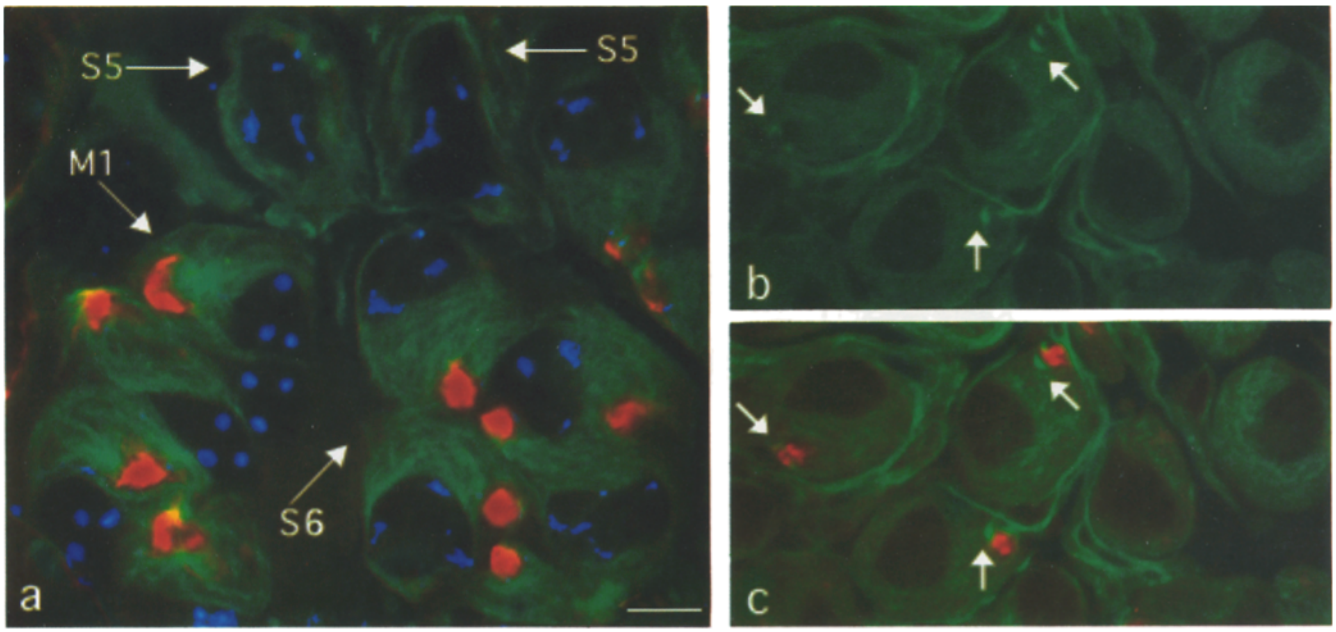

Figure 10. Actin behavior in *twinstar* mutant primary spermatocytes through prophase/prometaphase (stages S5 to M1). Pseudocolors as in Fig. 9. (*a*) Partial cyst containing S5, S6 and M1 mutant primary spermatocytes. Note that F-actin clusters are absent in S5 mature spermatocytes, but are prominent in S6 spermatocytes and in M1 prometaphase cells (type 1 aggregates). (*b* and *c*) S6 stage primary spermatocytes visualized with anti-tubulin antibodies (*b*) show the nascent asters in a particularly favorable preparation (*arrows*). The same field is shown in *c* with both anti-tubulin antibodies and rhodamine-labeled phalloidin to show association of type 1 actin aggregates with nascent asters. Bar, 10 μm.

Discussion

Structural Features of the twinstar Protein

Based on primary sequence similarity, the relatedness of the twinstar protein to known members of the cofilin/ADF family of actin severing/depolymerizing factors is unambiguous. Furthermore, preliminary biochemical data (Dr. S. K. Maciver, MRC, Cambridge, England, personal communication) have shown that bacterially expressed twinstar protein is able to bind and sever actin filaments, and that these activities are comparable to those of other previously characterized cofilins. Thus, twinstar protein behaves in vitro in a manner that is consistent with expectation. This implies that the functionality of conserved domains known to be important for actin binding and depolymerizing activities is retained in twinstar.

The structural features that govern the biochemical activities of cofilin-like proteins have not been completely characterized, nor is it clear how the different properties displayed by these proteins influence actin dynamics in different cellular environments. As one illustration, why certain cofilins show pH-dependent activity is not known, but it is thought that this feature might contribute to cytoskeletal changes seen upon alkalinization of the cytoplasm in response to cell activation by growth factors (see Sun et al., 1995). Nonetheless, several conserved motifs present in cofilin-like proteins are clearly implicated in specialized functions that may influence their activities. For example, one of the actin-binding domains identified in vertebrate homologues (Fig. 8, *filled bar*), which is well conserved in twinstar, competes with tropomyosin for binding to actin in vitro. This region may underlie the ability of vertebrate cofilins to compete for actin binding with tropomyosin, myosin, and villin headpiece in vitro (Nishida, et al., 1984; Nishida et al., 1985; Pope et al., 1994). We might therefore expect to find that twinstar also displays similar activities, which could be important for its function in vivo.

In addition, the actin depolymerizing activities of mammalian cofilin and destrin/ADF, yeast cofilin, and *Acanthamoeba* actophorin are specifically inhibited by certain phosphoinositides, which bind cofilin and displace it from actin (Yonezawa et al., 1990, 1991*b*; Iida et al., 1993; Moon et al., 1993; Quirk et al., 1993). Phospholipid binding may help maintain proteins near the plasma membrane and could potentially be involved in regulating their activity in vivo. One of the motifs present in cofilins that is known to bind actin is also critical for phospholipid binding (Fig. 8, *shaded bar*). This same motif also influences the ability of cofilin to inhibit hydrolysis of phospholipids by phospholipase C (Yonezawa et al., 1991*a,b*), an important enzyme linking phospholipid metabolism with cellular signaling cascades. We do not know whether twinstar activity is influenced by phosphoinositides, but based on the wide range of organisms in which this property is retained, the possibility seems likely. Other actin-binding proteins such as profilin and gelsolin also interact specifically with certain phosphoinositides (Lassing and Lindberg, 1985, 1988; Janmey and Stossel, 1987). However, the interaction of cofilins with phosphoinositides appears to be of both lower affinity and specificity than that of profilin, and the relevance of this feature in vivo remains to be established.

Finally, mammalian and avian cofilins and ADFs contain a motif, PXXXKKRKK (Fig. 8, *hatched bar*), that is very similar to the nuclear localization signal sequence of SV-40 large T antigen (Matsuzaki, et al., 1988). This se-

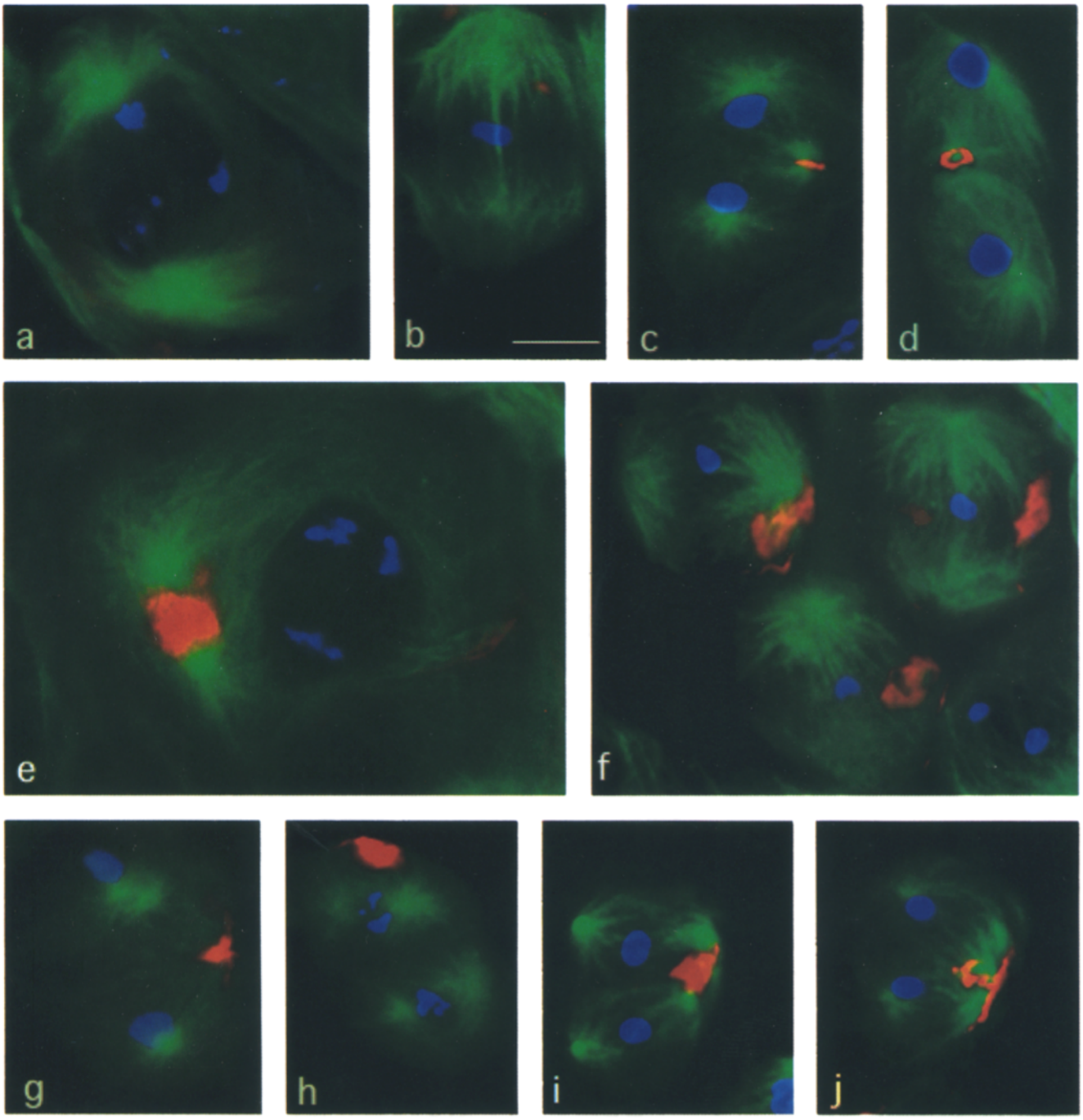

Figure 11. Actin behavior in wild-type and *twinstar* mutant spermatocytes from prometaphase through the completion of meiosis (stages M1 to M11). *a–d* are from Oregon R control testes; *e–j* are from tsr^1/tsr^1 males. Pseudocolors as in Fig. 9. (*a*) Late prophase I (stage M1a) and (*b*) metaphase I (stage M3) wild-type primary spermatocytes without prominent actin structures. (*c* and *d*) Telophase I cells at the M5 stage showing contractile actomyosin rings at the central spindle midzones. Depending upon the angle of observation, these structures either appear as bars (*c*) or exhibit a circular shape (*d*). (*e*) Mutant tsr^1/tsr^1 primary spermatocyte at the M1 stage, showing a prominent type 1 aggregate; compare with *a* of this figure. (*f*) Three metaphase I figures in the M3 stage associated with actin clusters (type 1 aggregates); compare with *b* of this figure. (*g*) A telophase I (M5 stage) showing a prominent and abnormally shaped actin ring (type 2 aggregate); compare with *c* and *d* of this figure. (*h*) Two secondary spermatocytes at late prometaphase (M8 stage) showing a single actin cluster associated with one of these cells. Most likely this is a type 2 aggregate that persists due to a failure in actin ring disassembly during telophase I. (*i*) Two metaphase II figures at the M9 stage showing a single actin aggregate. This structure is located in the same area occupied by the telophase I midbody, supporting the conclusion that it is a type 2 aggregate that originates from the actin ring. (*j*) A telophase II at the M11 stage with a clearly abnormal actin structure (type 3 aggregate) at the central spindle midzone. Bar, 10 μm.

quence is required in vertebrates for the translocation of cofilin into the nucleus upon heat shock or treatment with 10% DMSO (Nishida et al., 1987; Iida et al., 1992). Translocation is thought to be regulated by the phosphorylation state of a serine residue immediately upstream of this motif (Ohta et al., 1989; see Morgan et al., 1993). Twinstar retains distinct homology to the nuclear localization motif, while other nonvertebrate homologues retain only weak similarities; yeast cofilin is unable to localize to the nucleus (Moon et al., 1993). Based on sequence similarity, it seems possible that twinstar could translocate into the nucleus; however, it does not have a serine residue in exactly the same position relative to the signal sequence. We have no direct evidence at present to establish whether the twinstar protein can also translocate into the nucleus when *Drosophila* cells are stressed.

Actin Behavior in twinstar Mutants

Our observations provide strong evidence that actin dynamics are significantly perturbed in the absence of *tsr* activity. Staining with phalloidin, which specifically binds filamentous actin (Estes et al., 1981), shows that *tsr* testes contain large F-actin structures that are not seen in wild-type. Type 1 aggregates are first detected during the last stage of primary spermatocyte growth (stage S6) and then grow to reach their maximum size at the onset of the first meiotic division. We hypothesize that centrosomes serve as the foci for this abnormal accumulation of actin in mature primary spermatocytes because type 1 F-actin aggregates begin to form when nascent asters first become visible, and they remain associated with asters throughout prophase/prometaphase of meiosis I (M1 stage).

We speculate that a nucleation center for actin addition may exist near centrosomes in *tsr* mutants, and that the absence of twinstar activity may lead to uncontrolled actin accumulation at this site. Although phalloidin staining does not reveal the presence of F-actin in the vicinity of centrosomes in wild-type primary spermatocytes (data not shown), the actin-related protein Arp1 (also known as centractin or actin-RPV) has been found in association with centrosomes in other systems (Clark and Meyer, 1992; Lees-Miller et al., 1992). Arp1 forms a short F-actin-like filament that is part of the dynactin complex (Paschal et al., 1993; Schafer et al., 1994), which stimulates minus end-directed dynein-mediated vesicle motility along microtubules (Gill et al., 1991; Schroer and Sheetz, 1991). It is conceivable that a dynactin-like complex may normally localize to centrosomes in primary spermatocytes. Alternatively, if in *tsr* mutants the normal cytoplasmic or cortical anchors for a dynactin-like complex were disrupted, it could be pulled to the centrosome by its associated motor activity. In either case, this type of complex might provide a centrosomal focus for aberrant actin accumulation.

Unusual F-actin foci are also present in secondary spermatocytes and spermatids of *tsr* mutants (type 2 and type 3 aggregates), and almost certainly result from a failure to disassemble the actin structures found during telophase at the positions of the meiosis I and II contractile rings. Scrutiny of a large number of *tsr* meiotic cysts clearly shows that these telophase structures are more prominent than wild-type contractile rings and exhibit protuberances oriented along the spindle axis. During late telophase, these irregular rings do not disassemble as do normal contractile rings, but instead grow slightly larger and change morphology, becoming compact masses of F-actin. Type 2 actin aggregates eventually disappear during anaphase II in secondary spermatocytes, but then F-actin reassembles into a contractile ring-like structure (type 3 aggregate) during telophase II. Derivatives of this structure appear to persist as aggregates in spermatids that gradually disassemble during the elongation process.

We interpret the aberrant structures in secondary spermatocytes and spermatids as indicating that in *tsr* mutants, actin can assemble at the correct times and sites required for formation of the contractile ring. However, these actin assemblies are improperly organized, may be unable to function in cytokinesis, and fail to disassemble on a normal schedule. The eventual disassembly of aberrant actin aggregates may be mediated either by residual *tsr* activity in the mutants (neither tsr^1 nor tsr^2 is a null allele), or by the presence of other actin depolymerizing agents. Interestingly, the ribbon-like actin structure in young primary spermatocytes that we interpret as the male fusome degrades normally in *twinstar* mutants. This suggests that either disassembly of this structure does not depend on twinstar activity, or residual levels of twinstar protein at these earlier stages are sufficient for its disassembly.

In Vivo Functions of the twinstar Protein

Centrosome Migration and Separation. During both meiotic divisions in *tsr* mutants, in contrast with wild-type, the asters fail to associate with the nuclear envelope, and their migration to opposite poles is significantly delayed. That mutations in an actin binding protein result in such a phenotype is consistent with considerable precedent indicating an interaction between centrosomes and the actin cytoskeleton. In both yeast and nematodes, it appears that the establishment of correct spindle orientations involves a tethering of microtubules emanating from the centrosomes to specific sites on the actin cytoskeleton (Hyman and White, 1987; Hyman, 1989; Palmer et al., 1992; Waddle et al., 1994). Interestingly, in *S. cerevisiae* mutations in Arp1 homologues (Clark and Meyer, 1994; Muhua et al., 1994), dynein heavy chain (Eshel et al., 1993; Li et al., 1993), or actin, as well as mutations in β-tubulin that cause preferential loss of astral microtubules (Palmer et al., 1992), all result in similar misorientations of the mitotic spindle.

Although our data clearly show that alterations in the actin cytoskeleton can interfere with centrosome migration and separation during male meiosis in *Drosophila*, further studies will be required to define the molecular mechanisms underlying these events. At present, we can envisage two possibilities. It is conceivable that centrosome movements normally depend upon the tethering of astral microtubules to cortical or perinuclear actin structures. If such actin structures were incorrectly assembled in *tsr* mutants, they may fail to capture astral microtubules, leading to defects in centrosome migration and separation. Alternatively, the abnormal concentration of actin around the centrosomes of primary spermatocytes in *twinstar* mutants may physically obstruct normal interactions required for these processes.

We have been impressed by the apparent normality of

spindle morphology and chromosome separation in mutant testes subsequent to the aberrant migration of asters during prophase/prometaphase of meiosis I. This argues that the meiotic spindle has considerable self-regulating properties, which may be related to the extended period of time (between 20 and 45 min) required for bivalents to achieve a stable bipolar configuration before anaphase onset in these cells (Church and Lin, 1985). This might provide sufficient time for the asters in *twinstar* mutants to migrate eventually to their proper position so that correct chromosome segregation can occur. Final aster positioning in the mutant is likely to be mediated, at least in part, by microtubule-kinetochore attachments that may provide positional signals to restore proper aster localization. We envision that lateral forces exerted between interdigitating microtubules emanating from the two poles also participate in centrosome separation.

Cytokinesis. Larvae carrying mutant *tsr* alleles clearly exhibit frequent failures of cytokinesis both in neuroblast cells and in male meiosis. At present we have no information regarding the primary cause of cytokinesis failure in neuroblasts. However, our observations on testes suggest two possible explanations for how a reduction in twinstar activity might affect meiotic cytokinesis.

The first possibility is that the cytokinesis defect arises primarily from the abnormal migration and positioning of asters. It is clear that mechanisms must exist that transmit signals from the spindle asters to the contractile apparatus, explaining how difficulties in cytokinesis could result indirectly from problems in centrosome positioning within the cell. A number of experiments indicate that the spindle asters specify the position of the cleavage furrow midway between them (reviewed by Rappaport, 1986), and some evidence suggests that the asters may be able to dictate this position as early as prophase (Sluder and Miller, 1990), when the irregularities in *twinstar* aster localization are manifested. We believe this possibility to be unlikely because *tsr* mutants correctly localize actin structures to the midzone at the same time that normal contractile rings form. Nevertheless, it remains conceivable that a putative alteration of signals emanating from the asters could affect the responsiveness of the cortical cytoplasm without affecting positioning of the contractile ring.

The more likely possibility is that cytokinesis is disrupted in *tsr* mutants because of abnormalities in the formation and/or disassembly of the contractile ring. Our observations clearly show that *tsr* mutants exhibit morphologically abnormal contractile rings that fail to disassemble during cleavage. Most current models of cytokinesis assert that the contractile ring is an overlapping array of actin filaments of opposite polarity attached to the plasma membrane. These actin filaments interact with bipolar myosin-II filaments, leading to constriction of the cell periphery (reviewed in Satterwhite and Pollard, 1992; Fishkind and Wang, 1995). One could easily imagine several scenarios by which a cofilin-like protein such as twinstar, which can modulate actin dynamics in vitro by severing and depolymerizing filaments (S. K. Maciver, personal communication), might play a role in cytokinesis. Such an activity might function in the recruitment of cortical actin filaments to the contractile ring (Cao and Wang, 1990), turnover of actin within the contractile ring (Inoue, 1990), or disassembly of the contractile ring during furrowing and cleavage (Maupin and Pollard, 1986). In any event, there is substantial precedent to suggest that the twinstar protein could function in concert with other proteins to promote proper organization of contractile filaments. The cofilin homologue actophorin, in the presence of the actin cross-linking protein α-actinin, promotes formation of actin bundles in vitro (Maciver, et al., 1991). In addition, the correct assembly of the contractile myofilament lattice in the body wall muscle of *C. elegans* requires an activity encoded by a cofilin-like gene: in *unc-60* mutants, thin filaments aggregate at the ends of the cell instead of interdigitating with thick filaments, which appear essentially normal (Waterston et al., 1980). Most recently, vertebrate cofilin has been found to localize to the contractile ring in tissue culture (Nagaoka et al., 1995).

Additional Functions of the twinstar Protein

We believe it unlikely that *twinstar* function is required only for cytokinesis or correct aster migrations in prophase. It is quite possible that the phenotypes we have examined represent only those events that are most susceptible to depletion of maternal twinstar protein stores. Neither the tsr^1 nor the tsr^2 allele appears to represent the null state of the *twinstar* locus: some mRNA is expressed in mutant animals and these mutations do not interfere with the open reading frame encoding the protein. Other functions of twinstar might therefore be uncovered by an analysis of phenotypes associated with either true null mutations, which can in theory be isolated by transposase-promoted imprecise excision of the tsr^1 or tsr^2 P elements (Bellen et al., 1989), or conditional mutations. We expect to find that twinstar protein may also be required for muscle formation, or for processes such as cellular motility or the determination of cell shape in *Drosophila*. In this light, it is interesting to note that when a *Drosophila* cDNA clone essentially identical to our *twinstar* cDNA is overexpressed in *S. pombe*, changes in cell shape are observed in association with perturbations in actin distribution (Edwards et al., 1994). Their results, in combination with the findings described in this paper, emphasize the importance to the cell of maintaining the proper stoichiometry of cofilin with respect to other cytoskeletal components.

The authors wish to thank kindly the following: Drs. Trish Wilson and Minx Fuller for donating the tsr^2 allele, Drs. K. Edwards and D. Kiehart for sharing sequence information before publication and for helpful comments on the protein alignment, Dr. Bruce Reed for stocks and information on complementation groups, Dr. S. K. Maciver for early communication of new biochemical data, Dr. J. Merriam for making a collection of P element-induced mutations available to us, Dr. H. Lin for helpful discussions about the fusome, E. Mirabile for participating in early stages of our screening procedure, and Janis Werner for microinjections.

This work was supported by National Institutes of Health grant 5R01GM48430 to M. L. Goldberg, by National Institutes of Health Training grant 5T32GM07617 to K. C. Gunsalus, and by grants to M. Gatti from Progetto Finalizzato Ingegneria Genetica and Fondazione Istituto Pasteur-Cenci Bolognetti.

Received for publication 17 May 1995 and in revised form 31 July 1995.

References

Abe, H., T. Endo, K. Yamamoto, and T. Obinata. 1990. Sequence of cDNAs

encoding actin depolymerizing factor and cofilin of embryonic chicken skeletal muscle: two functionally distinct actin-regulatory proteins exhibit high structural homology. *Biochemistry* 29:7420–7425.

Bamburg, J. R., and D. Bray. 1987. Distribution and cellular localization of actin depolymerizing factor. *J. Cell Biol.* 105:2817–2825.

Bellen, H. J., C. J. O'Kane, C. Wilson, U. Grossniklaus, R. K. Pearson, and W. J. Gehring. 1989. P element-mediated enhancer detection: a versatile method to study development in *Drosophila. Genes & Dev.* 3:1288–1300.

Bier, E., H. Vaessin, S. Shepherd, K. Lee, K. McCall, S. Barbel, L. Ackerman, R. Carretto, T. Uemura, E. Grell, L. Y. Jan, and Y. N. Jan. 1989. Searching for pattern and mutation in the *Drosophila* genome with a *P-lacZ* vector. *Genes & Dev.* 3:1273–1287.

Blose, S. H., D. I. Meltzer, and J. R. Feramisco. 1982. 10 nm filaments induced to collapse in cells microinjected with antibodies against tubulin. *J. Cell Biol.* 95:229a.

Brown, N. H., and F. C. Kafatos. 1988. Functional cDNA libraries from *Drosophila* embryos. *J. Mol. Biol.* 203:425–437.

Brown, N. H., D. L. King, M. Wilcox, and F. C. Kafatos. 1989. Developmentally regulated alternative splicing of *Drosophila* integrin PS2 alpha transcripts. *Cell.* 59:185–195.

Cao, L.-G., and Y.-L. Wang. 1990. Mechanism of formation of contractile ring in dividing cultured animal cells. II. Cortical movements of microinjected actin filaments. *J. Cell Biol.* 111:1905–1911.

Castrillon, D. H., and S. A. Wasserman. 1994. *diaphanous* is required for cytokinesis in *Drosophila* and shares domains of similarity with the products of the *limb deformity* gene. *Development (Camb.).* 120:3367–3377.

Cavener, D. R. 1987. Comparison of the consensus sequence flanking translational start sites in *Drosophila* and vertebrates. *Nucleic Acids Res.* 15:1353–1361.

Cenci, G., S. Bonaccorsi, C. Pisano, F. Verni, and M. Gatti. 1994. Chromatin and microtubule organization during premeiotic, meiotic and early postmeiotic stages of *Drosophila melanogaster* spermatogenesis. *J. Cell Sci.* 107: 3521–3534.

Chirgwin, J. M., A. E. Pyrzybyla, R. J. MacDonald, and W. J. Rutter. 1979. Isolation of biologically active ribonucleic acid from sources enriched in ribonuclease. *Biochemistry.* 18:5294–5299.

Cho, Y.-J., J. Liu, and S. E. Hitchcock-DeGregori. 1990. The amino terminus of muscle tropomyosin is a major determinant for function. *J. Biol. Chem.* 265: 538–545.

Church, K., and H. P. Lin. 1985. Kinetochore microtubules and chromosome movement during prometaphase in *Drosophila melanogaster* spermatocytes studied in life and with the electron microscope. *Chromosoma.* 92:273–282.

Clark, S. W., and D. I. Meyer. 1992. Centractin is an actin homologue associated with the centrosome. *Nature (Lond.).* 359:246–250.

Clark, S. W., and D. I. Meyer. 1994. *ACT3*: a putative centractin homologue in *S. cerevisiae* is required for proper orientation of the mitotic spindle. *J. Cell Biol.* 127:129–138.

Devereux, J., P. Haeberli, and O. Smithies. 1984. A comprehensive set of sequence analysis programs for the VAX. *Nucleic Acids Res.* 12:365–372.

Edwards, K. A., R. A. Montague, S. Shepard, B. A. Edgar, R. L. Erikson, and D. P. Kiehart. 1994. Identification of *Drosophila* cytoskeletal proteins by induction of abnormal cell shape in fission yeast. *Proc. Natl. Acad. Sci. USA.* 91:4589–4593.

Eshel, D., L. A. Urrestarazu, S. Vissers, J.-C. Jauniaux, J. C. v. Vliet-Reedijk, R. J. Planta, and I. R. Gibbons. 1993. Cytoplasmic dynein is required for normal nuclear segregation in yeast. *Proc. Natl. Acad. Sci. USA.* 90:11172–11176.

Estes, J. E., L. A. Selden, and L. C. Gershman. 1981. Mechanism of action of phalloidin on the polymerization of muscle actin. *Biochemistry.* 20:708–712.

Fishkind, D. J., and Y.-L. Wang. 1995. New horizons in cytokinesis. *Curr. Opin. Cell Biol.* 7:23–31.

Fuller, M. T. 1993. Spermatogenesis. *In* The Development of Drosophila Melanogaster. Vol. I. M. Bate and A. M. Arias, editors. Cold Spring Harbor Laboratory Press, Plainview, NY. 71–147.

Gatti, M., and B. S. Baker. 1989. Genes controlling essential cell-cycle functions in *Drosophila. Genes & Dev.* 3:438–453.

Gatti, M., and M. L. Goldberg. 1991. Mutations affecting cell division in *Drosophila. Methods Cell Biol.* 35:543–586.

Gill, S. R., T. A. Schroer, I. Szilak, E. R. Steuer, M. P. Sheetz, and D. W. Cleveland. 1991. Dynactin, a conserved, ubiquitously expressed component of an activator of vesicle motility mediated by cytoplasmic dynein. *J. Cell Biol.* 115:1639–1650.

Glover, D. M. 1989. Mitosis in *Drosophila. J. Cell Sci.* 92:137–146.

González, C., J. Casal, and P. Ripoll. 1989. Relationship between chromosome content and nuclear diameter in early spermatids of *Drosophila melanogaster. Genet. Res. Camb.* 54:205–212.

Gubb, D., S. McGill, and M. Ashburner. 1988. A selective screen to recover chromosomal deletions and duplications in *Drosophila melanogaster. Genetics.* 119:377–390.

Hawkins, M., B. Pope, S. K. MacIver, and A. G. Weeds. 1993. Human actin depolymerizing factor mediates a pH-sensitive destruction of actin filaments. *Biochemistry.* 32:9985–9993.

Hayden, S. M., P. S. Mille, A. Brauweiler, and J. R. Bamburg. 1993. Analysis of the interactions of actin depolymerizing factor with G- and F-actin. *Biochemistry.* 32:9994–10004.

Hyman, A. A. 1989. Centrosome movement in the early divisions of *Caenorhabditus elegans*: a cortical site determining centrosome position. *J. Cell Biol.* 109:1185–1193.

Hyman, A. A., and J. G. White. 1987. Determination of cell division axes in the early embryogenesis of *Caenorhabditus elegans. J. Cell Biol.* 105:2123–2135.

Iida, K., S. Matsumoto, and I. Yahara. 1992. The KKRKK sequence is involved in heat shock-induced nuclear translocation of the 18-kDa actin-binding protein, cofilin. *Cell Struct. Funct.* 17:39–46.

Iida, K., K. Moriyama, S. Matsumoto, H. Kawasaki, E. Nishida, and I. Yahara. 1993. Isolation of a yeast essential gene, *COF1*, that encodes a homologue of mammalian cofilin, a low-M_r actin-binding and depolymerizing protein. *Gene (Amst.).* 124:115–120.

Inoue, S. 1990. Dynamics of mitosis and cleavage. *Annu. NY Acad. Sci.* 582:1–14.

Janmey, P. A., and T. P. Stossel. 1989. Gelsolin-phosphoinositide interaction. Full expression of gelsolin-inhibiting function by polyphosphoinositides in vesicular form and inactivation by dilution, aggregation, or masking of the inositol head group. *J. Biol. Chem.* 264:4825–4831.

Karess, R. E., X.-J. Chang, K. A. Edwards, S. Kukarni, I. Aguilera, and D. P. Kiehart. 1991. The regulatory light chain of nonmuscle myosin is encoded by *spaghetti-squash*, a gene required for cytokinesis in *Drosophila. Cell.* 65: 1177–1189.

Ketchum, A. S., C. T. Stewart, M. Stewart, and D. Kiehart. 1990. Complete sequence of the *Drosophila* nonmuscle myosin heavy-chain transcript: conserved sequences in the myosin tail and differential splicing in the 5′-untranslated sequence. *Proc. Natl. Acad. Sci. USA.* 87:663–667.

Kim, S.-R., Y. Kim, and G. An. 1993. Molecular cloning and characterization of anther-preferential cDNA encoding a putative actin-depolymerizing factor. *Plant Mol. Biol.* 21:39–45.

Klemenz, R., U. Weber, and W. J. Gehring. 1987. The *white* gene as a maker in a new P-element vector for gene transfer in *Drosophila. Nucleic Acids Res.* 15:3947–3959.

Lassing, I., and U. Lindberg. 1985. Specific interaction between phosphatidylinositol 4,5 bisphosphate and and profilactin. *Nature (Lond.).* 314:472–474.

Lassing, I., and U. Lindberg. 1988. Specificity of the interaction between phosphatidylinositol 4,5-bisphosphate and the profilin:actin complex. *J. Cell. Biochem.* 37:255–267.

Lees-Miller, J. P., D. M. Helfman, and T. A. Schroer. 1992. A vertebrate actin-related protein is a component of a multisubunit complex involved in microtubule-based vesicle motility. *Nature (Lond.).* 359:244-246.

Li, Y. Y., E. Yeh, T. Hays, and K. Bloom. 1993. Disruption of mitotic spindle orientation in a yeast dynein mutant. *Proc. Natl. Acad. Sci. USA.* 90:10096–11000.

Lin, H., L. Yue, and A. C. Spradling. 1994. The *Drosophila* fusome, a germline-specific organelle, contains membrane skeletal proteins and functions in cyst formation. *Development (Camb.).* 120:947–956.

Lindsley, D. L., and G. G. Zimm. 1992. The genome of *Drosophila melanogaster.* Academic Press, Inc., San Diego, CA. 1133 pp.

Maciver, S. K., D. H. Wachsstock, W. H. Schwarz, and T. D. Pollard. 1991. The actin filament severing protein actophorin promotes the formation of rigid bundles of actin filaments cross-linked with α-actinin. *J. Cell Biol.* 115:1621–1628.

Matsuzaki, F., S. Matsumoto, I. Yahara, N. Yonezawa, E. Nishida, and H. Sakai. 1988. Cloning and characterization of porcine brain cofilin cDNA. *J. Biol. Chem.* 263:11564–11568.

Maupin, P., and T. D. Pollard. 1986. Arrangement of actin filaments and myosin-like filaments in the contractile ring and of actin-like filaments in the mitotic spindle of dividing HeLa cells. *J. Ultrastruct. Mol. Struct. Res.* 94:92–103.

McKim, K. M., C. Matheson, M. A. Marra, M. F. Wakarchuk, and D. L. Baillie. 1994. The *Caenorhabditus elegans unc-60* gene encodes proteins homologous to a family of actin binding proteins. *Mol. Gen. Genet.* 242:346–357.

McKim, K. S., M. F. P. Heschl, R. E. Rosenbluth, and D. L. Baillie. 1988. Genetic organization of the *unc-60* region in *Caenorhabditus elegans. Genetics.* 118:49–59.

Moon, A. L., P. A. Janmey, K. A. Louie, and D. G. Drubin. 1993. Cofilin is an essential component of the yeast cortical cytoskeleton. *J. Cell Biol.* 120:421–435.

Morgan, T. E., R. O. Lockerbie, L. S. Minamide, M. D. Browning, and J. R. Bamburg. 1993. Isolation and characterization of a regulated form of actin depolymerizing factor. *J. Cell Biol.* 122:623–633.

Moriyama, K., S. Matsumoto, E. Nishida, H. Sakai, and I. Yahara. 1990*a*. Nucleotide sequence of mouse cofilin cDNA. *Nucleic Acids Res.* 18:3053.

Moriyama, K., E. Nishida, N. Yonezawa, H. Sakai, S. Matsumoto, K. Iida, and I. Yahara. 1990*b*. Destrin, a mammalian actin-depolymerizing protein, is closely related to cofilin. *J. Biol. Chem.* 265:5768–5773.

Moriyama, K., N. Yonezawa, H. Sakai, I. Yahara, and E. Nishida. 1992. Mutational analysis of an actin-binding site of cofilin and characterization of chimeric proteins between cofilin and destrin. *J. Biol. Chem.* 267:7240–7244.

Mount, S. M. 1982. A catalogue of splice junction sequences. *Nucleic Acids Res.* 10:459–472.

Muhua, L., T. S. Karpova, and J. A. Cooper. 1994. A yeast actin-related protein homologous to that in vertebrate dynactin complex is important for spindle orientation and nuclear migration. *Cell.* 78:669–679.

Nagaoka, R., H. Abe, K. I. Kusano, and T. Obinata. 1995. Concentration of co-

filin, a small actin-binding protein, at the cleavage furrow during cytokinesis. *Cell Motil. Cytoskel.*30:1–7.

Neufeld, T. P., and G. M. Rubin. 1994. The *Drosophila peanut* gene is required for cytokinesis and encodes a protein similar to yeast putative bud neck filament proteins. *Cell.* 77:371–379.

Nishida, E., S. Maekawa, and H. Sakai. 1984. Cofilin, a protein in porcine brain that binds to actin filaments and inhibits their interactions with myosin and tropomyosin. *Biochemistry.* 23:5307–5313.

Nishida, E., E. Muneyuki, S. Maekawa, Y. Ohta, and H. Sakai. 1985. An actin-depolymerizing protein (destrin) from porcine kidney. Its action on F-actin containing or lacking tropomyosin. *Biochemistry* 24:6624–6630.

Nishida, E., S. Maekawa, E. Muneyuke, and H. Sakai. 1987. Cofilin is a component of intranuclear and cytoplasmic actin rods induced in cultured cells. *Proc. Natl. Acad. Sci. USA.* 84:5262–5266.

O'Connell, P., and M. Rosbash. 1984. Sequence, structure, and codon preference of the *Drosophila* ribosomal protein 49 gene. *Nucleic Acids Res.* 12: 5495–5513.

O'Kane, C. J., and W. J. Gehring. 1987. Detection *in situ* of genomic regulatory elements in *Drosophila. Proc. Natl. Acad. Sci. USA.* 84:9123–9127.

Ochman, H., A. S. Gerber, and D. L. Hartl. 1988. Genetic applications of an inverse polymerase chain reaction. *Genetics.* 120:621–624.

Ogawa, K., M. Tashima, Y. Yumoto, T. Okuda, H. Sawada, M. Okuma, and Y. Maruyama. 1990. Coding sequence of human placenta cofilin cDNA. *Nucleic Acids Res.* 18:7169.

Ohta, Y., E. Nishida, H. Sakai, and E. Miyamoto. 1989. Dephosphorylation of cofilin accompanies heat shock-induced nuclear accumulation of cofilin. *J. Biol. Chem.* 264:16143–16148.

Palmer, R. E., D. S. Sullivan, T. Huffaker, and D. Koshland. 1992. Role of astral microtubules and actin in spindle orientation and migration in the budding yeast, *Saccharomyces cerevisiae. J. Cell Biol.* 119:583–593.

Paschal, B. M., E. L. F. Holzbaur, K. K. Pfister, S. Clark, and D. I. Meyer. 1993. Characterization of a 50-kDa polypeptide in cytoplasmic dynein preparations reveals a complex with $p150^{Glued}$ and a novel actin. *J. Biol. Chem.* 268: 15318–15323.

Pearson, W. R., and D. J. Lipman. 1988. Improved tools for biological sequence comparison. *Proc. Natl. Acad. Sci. USA.* 85:2444–2448.

Pirotta, V. 1986. Cloning *Drosophila* genes. *In* Drosophila: A Practical Approach. D. B. Roberts, editor. IRL Press, Oxford. 83–110.

Pope, B., M. Way, P. T. Matsudaira, and A. Weeds. 1994. Characterization of the F-actin binding domains of villin: classification of F-actin binding proteins into two groups according to their binding sites on actin. *FEBS Lett.* 338:58–62.

Quirk, S., S. K. Maciver, C. Ampe, S. K. Doberstein, D. A. Kaiser, J. Van-Damme, J. S. Vandekerckhove, and T. D. Pollard. 1993. Primary structure of and studies on *Acanthamoeba actophorin. Biochemistry.* 32:8525–8533.

Rappaport, R. 1986. Establishment of the mechanism of cytokinesis in animal cells. *Intl. Rev. Cytol.* 105:245-281.

Ripoll, P., J. Casal, and C. Gonzalez. 1987. Towards the genetic dissection of mitosis in *Drosophila. Bioessays.* 7:204–210.

Robertson, H. M., C. R. Preston, R. W. Phillips, D. M. Johnson-Schlitz, W. K. Benz, and W. R. Gehring. 1988. A stable source of P element transposase in *Drosophila melanogaster. Genetics.* 118:461–470.

Rose, L. S., and E. Weischaus. 1992. The *Drosophila* cellularization gene *nullo* produces a blastoderm-specific transcript whose levels respond to the nucleocytoplasmic ratio. *Genes & Dev.* 6:1255–1268.

Sambrook, J., E. F. Fritsch, and T. Maniatis. 1989. Molecular Cloning: A Laboratory Manual. Vol. 1–3. Cold Spring Harbor Laboratory Press, Cold Spring Harbor, New York.

Sanger, F., S. Nicklen, and I. R. Coulson. 1977. DNA sequencing with chain-terminating inhibitors. *Proc. Natl. Acad. Sci. USA.* 74:5463–5467.

Satterwhite, L. L., and T. D. Pollard. 1992. Cytokinesis. *Curr. Opin. Cell Biol.* 4: 43-52.

Schafer, D. A., S. R. Gill, J. A. Cooper, J. E. Heuser, and T. A. Schroer. 1994. Ultrastructural analysis of the dynactin complex: an actin-related protein is a component of a filament that resembles F-actin. *J. Cell Biol.* 126:403–412.

Schroer, T. A., and M. P. Sheetz. 1991. Two activators of microtubule-based vesicle transport. *J. Cell Biol.* 115:1309–1318.

Simpson, P. 1983. Maternal-zygotic gene interactions during formation of the dorsoventral pattern in *Drosophila* embryos. *Genetics.* 105:615–632.

Sluder, G., and F. J. Miller. 1990. What determines when the cleavage furrow is formed? *Annu. NY Acad. Sci.* 582:308–309.

Sun, H.-Q., K. Kwiatkowska, and H. L. Yin. 1995. Actin monomer binding proteins. *Curr. Opin. Cell Biol.* 7:102–110.

Tates, A. D. 1971. Cytodifferentiation during spermatogenesis in *Drosophila melanogaster*: an electron microscope study. Ph.D. thesis, Rijksuniversiteit, Leiden.

Vandekerckhove, J., and K. Vancompernolle. 1992. Structural relationships of actin binding proteins. *Curr. Opin. Cell Biol.* 4:41–50.

Waddle, J. A., J. A. Cooper, and R. H. Waterson. 1994. Transient localized accumulation of actin in *Caenorhabditus elegans* blastomeres with oriented asymmetric divisions. *Development (Camb.).* 120:2317–2328.

Waterston, R. H., J. N. Thomson, and S. Brenner. 1980. Mutants with altered muscle structure in *Caenorhabditus elegans. Dev. Biol.* 77:271–302.

Yonezawa, N., E. Nishida, K. Iida, I. Yahara, and H. Sakai. 1989. An actin-interacting heptapeptide in the cofilin sequence. *Eur. J. Biochem.* 183:235–238.

Yonezawa, N., E. Nishida, K. Iida, I. Yahara, and H. Sakai. 1990. Inhibition of the interactions of cofilin, destrin, and deoxyribonuclease I with actin by phosphoinositides. *J. Biol. Chem.* 265:8382–8386.

Yonezawa, N., E. Nishida, and H. Sakai. 1985. pH control of actin polymerization by cofilin. *J. Biol. Chem.* 260:14410–14412.

Yonezawa, N., E. Nishida, K. Iida, H. Kumagai, I. Yahara, and H. Sakai. 1991*a*. Inhibition of actin polymerization by a synthetic dodecapeptide patterned on the sequence around the actin-binding site of cofilin. *J. Cell Biol.* 266: 10485–10489.

Yonezawa, N., Y. Homma, I. Yahara, H. Sakai, and E. Nishida. 1991*b*. A short sequence responsible for both phosphoinositide binding and actin binding activities of cofilin. *J. Biol. Chem.* 266:17218–17221.